

1 **A 20-year study of melt processes over Larsen C Ice Shelf using a high-resolution**
2 **regional atmospheric model: Part 2, Drivers of surface melting**

3

4 E. Gilbert^{1,2, †}, A. Orr¹, I. A. Renfrew², J. C. King¹, and T. Lachlan-Cope¹

5

6 ¹ British Antarctic Survey, High Cross, Madingley Road, Cambridge CB3 0ET, United
7 Kingdom.

8 ² School of Environmental Sciences, University of East Anglia, Norwich NR4 7TJ, United
9 Kingdom.

10

11 Corresponding author: Ella Gilbert (ella.gilbert@reading.ac.uk)

12

13 † Present address: Department of Meteorology, University of Reading, Whiteknights Road,
14 Reading RG6 6ET, United Kingdom.

15

16 **Key words:** Larsen C ice shelf; Antarctic Peninsula; regional climate modelling; surface
17 melt; meteorology; model hindcast

18

19 **Key points:**

- 20
- The amount of surface melting on Larsen C is driven mostly by sunny conditions,
21 followed by foehn events, cloud and large-scale circulation
 - Deep Amundsen Sea Low, positive Southern Annular Mode, and El Niño conditions
22 enhance surface melting
 - Drivers of surface melting overlap and interact
- 23
24
25
26

27

27 **Abstract**

28 Quantifying the relative importance of the atmospheric drivers of surface melting on the
29 Larsen C ice shelf is critical in the context of recent and future climate change. Here, we
30 present analysis of a new multi-decadal, high-resolution model hindcast using the Met Office
31 Unified Model (MetUM), described in part 1 of this study. We evaluate the contribution of
32 various atmospheric conditions in order to identify and rank, for the first time, the most
33 significant causes of melting over the recent past. We find the primary driver of surface
34 melting on Larsen C is solar radiation. Foehn events are the second most important

35 contributor to surface melting, especially in non-summer seasons when less solar radiation is
36 received at the surface of the ice shelf. Thirdly, cloud influences surface melting via its
37 impact on the surface energy balance (SEB); when the surface temperature is warm enough,
38 cloud can initiate or prolong periods of melting. Lastly, large-scale circulation patterns such
39 as the Southern Annular Mode (SAM), El Niño Southern Oscillation (ENSO) and Amundsen
40 Sea Low (ASL) control surface melting on Larsen C by influencing the local meteorological
41 conditions and SEB. These drivers of melting interact and overlap, for example, the SAM
42 influences the frequency of foehn, commonly associated with leeside cloud clearances and
43 sunnier conditions. Ultimately, these drivers matter because sustained surface melting on
44 Larsen C could destabilise the ice shelf via hydrofracturing, which would have consequences
45 for the fate of the ice shelf and sea levels worldwide.

46

47 **Plain Language Summary**

48

49 In order to predict the future of the largest remaining ice shelf on the Antarctic Peninsula -
50 Larsen C – we must understand what is causing it to melt at the surface. We use results from
51 a new model dataset to explore which causes of melting are the most important. Our results
52 show that the most dominant factor is solar radiation, especially in summer, while relatively
53 warm, dry foehn winds are the second most important cause of melting. Foehn winds are an
54 especially significant cause of melting in non-summer seasons. The third driver of surface
55 melting is cloud, because clouds can affect how much energy is received at the surface of the
56 ice shelf. When it is warm enough, clouds can initiate or sustain melting. The final cause of
57 melting is large-scale atmospheric circulation patterns, which can establish the conditions
58 that promote melting, such as sunny, cloudy or foehn periods. These melt drivers interact
59 with one another and can compound or dampen the effects of other causes of melting. These
60 melt drivers matter because surface melt could cause this ice shelf to collapse, and therefore
61 indirectly contribute to sea level rise.

62

63

64 **1 Introduction**

65

66 Atmospheric drivers of surface melting were implicated in the collapse of the Larsen A and B
67 ice shelves that previously neighboured Larsen C - the largest remaining ice shelf on the
68 eastern side of the Antarctic Peninsula and which extends north of the Antarctic circle - by

69 increasing firn densification, meltwater ponding and ultimately hydrofracturing and
70 disintegration (Scambos et al., 2000; 2003; Bell et al., 2018). In particular, the large-scale
71 circumpolar westerly circulation is known to have an important role in the Antarctic
72 Peninsula region by influencing local atmospheric conditions via its effect on foehn winds.
73 Foehn winds cause leeside warming and associated melting over these ice shelves (van
74 Lipzig et al., 2008; Orr et al., 2008; 2021; Cape et al., 2015; Elvidge et al. 2015, 2016; King
75 et al. 2017; Kuipers Munneke et al., 2018), and a distinct west-east gradient in melting over
76 Larsen C (Bevan et al., 2018; Elvidge et al. 2020; Gilbert et al., 2022). Large-scale
77 circulation variability in the Southern Hemisphere is strongly influenced by the Southern
78 Annular Mode (SAM). The SAM underwent a positive trend from the 1960s to the mid-
79 1990s, particularly in austral summer (December, January, February; DJF), causing flow to
80 be more dominantly westerly (Marshall, 2003; Marshall et al., 2006; Fogt & Marshall, 2020),
81 although there has not been a significant trend since then. Stronger westerly flow associated
82 with a more positive SAM strengthened the flow impinging on the Antarctic Peninsula,
83 resulting in increased foehn-induced warming over the ice shelves (Orr et al., 2008; Cape et
84 al., 2015; Datta et al., 2019).

85

86 The SAM is strongly correlated with the strength of the Amundsen Sea Low (ASL), which is
87 a climatological low-pressure centre in the Amundsen/Bellingshausen Seas to the west of the
88 Antarctic Peninsula. The ASL influences near-surface wind, temperature and sea ice
89 concentration, and thus primarily temperatures on the western side of the Antarctic Peninsula
90 (King, 1994; Turner et al., 2013; Hosking et al., 2013). The El Niño Southern Oscillation
91 (ENSO) teleconnection also influences the ASL, primarily during austral winter (June, July,
92 August; JJA) and spring (September, October, November; SON) (Clem et al., 2016). The
93 SAM and ENSO are shown to be anti-correlated throughout the instrumental record (Fogt et
94 al., 2011; Dätwyler et al., 2020), and by influencing the strength of the ASL can affect the
95 advection of warm maritime air across the Antarctic Peninsula and thus atmospheric
96 conditions (including foehn events) over its eastern side.

97

98 The high mountains (~2000 m) running along the spine of the Antarctic Peninsula present a
99 significant barrier separating the relatively warm, maritime environment to the west from a
100 much cooler continental climate on the eastern side (Orr et al., 2004). As well as acting as a
101 barrier to prevailing westerly winds, cold air masses on the eastern side of the Antarctic
102 Peninsula can also be blocked by the high orography, resulting in the formation of strong

103 southerly or ‘barrier’ winds flowing along the eastern side of the Peninsula (Schwerdtfeger,
104 et al. 1975; Parish, 1983), which can therefore affect temperatures over Larsen C.

105

106 Regional climate models (RCMs) are commonly used to assess the role of atmospheric
107 drivers of melt on Larsen C due to the dearth of long-term observations (e.g. Orr et al., 2008,
108 2021; Elvidge et al., 2015; 2016; 2020; Turton et al., 2018; 2020; Kuipers Munneke et al.,
109 2018; Wiesenekker et al., 2018; Datta et al., 2019; Laffin et al., 2021; Gilbert et al., 2022).
110 However, many of these studies have focused on particular meteorological phenomena,
111 especially the role of foehn winds (e.g. Turton et al., 2018; 2020; Datta et al., 2019; Laffin et
112 al., 2021; Orr et al., 2021), and/or have examined melt over a relatively short timeframe (e.g.
113 Kuipers Munneke et al., 2018; Gilbert et al., 2020; Elvidge et al., 2016; 2020). To date, no
114 work has attempted to assess the relative importance of the first-order drivers of surface
115 melting on Larsen C (i.e., SW radiation, foehn, cloud cover and phase, and large-scale
116 circulation patterns like the SAM, ENSO and ASL) on the surface energy balance (SEB) or
117 melting over a multi-decadal time period.

118

119 While van Wessem et al. (2015; 2016) produced near-surface climatologies of winds /
120 temperatures and surface mass balance, respectively, over the Antarctic Peninsula using
121 RACMO2.3 (Regional Atmospheric Climate Model) at a spatial resolution of 5.5 km,
122 “significant biases” remained that the authors attribute to difficulties in resolving the steep
123 topography that characterises the region (van Wessem et al., 2016: p271). Resolving complex
124 topography is vital for realistically simulating foehn winds, and may be more difficult using
125 RACMO2.3 because its hydrostatic core prohibits the use of kilometre scale spatial resolution
126 (Orr et al., 2021). It should be noted, however, that Weisenekker et al. (2018) and Laffin et
127 al. (2021) highlight RACMO2.3’s satisfactory ability to resolve foehn events over Larsen C.
128 Wiesenekker et al. (2018) diagnose foehn wind occurrence between 1979-2016 at Cabinet
129 Inlet on Larsen C, situated close to the foot of the eastern slopes of the Antarctic Peninsula,
130 from AWS and RACMO2.3 model data, but do not relate this to the SEB. King et al. (2015)
131 comprehensively evaluate the ability of three RCMs to reproduce observed meteorology and
132 SEB on Larsen C during summer 2010/11, but the period is short – just one month. Gilbert et
133 al. (2020) evaluate melting on Larsen C over this same one-month period but focus solely on
134 the role of cloud on melt. Similarly, Elvidge et al. (2020) use the regional configuration of the
135 UK Met Office Unified Model (MetUM) at 1.5 km resolution to assess the role of various
136 SEB regimes in driving melt on Larsen C and include a thorough investigation of the role of

137 solar radiation and foehn and the conditions that produce these, but this process-focused
138 study is limited in its duration to six months. Datta et al. (2019) use the MAR (Modèle
139 Atmosphérique Régionale) model at 7.5 km resolution to evaluate the effect of foehn events
140 on the evolution of the snowpack during the period 1982-2017 and find three regimes in
141 which surface melting occurs, related to foehn winds and cloud occurrence. However, the
142 focus of their study is on the evolution of firn and the snowpack, rather than quantifying the
143 atmospheric processes that influence the SEB regime and surface melting. Laffin et al. (2021)
144 examine the impact of foehn winds on melting during 1979–2018 using machine learning and
145 the RACMO2.3 model, and Turton et al. (2020) combine observations and model output
146 from AMPS (Antarctic Mesoscale Prediction System) to explore seasonal patterns in foehn-
147 driven surface melt. Lastly, Bozkurt et al. (2020) use the WRF (Weather Research and
148 Forecasting) model at 15 km resolution to produce a hindcast for the Antarctic Peninsula over
149 the period 1991-2015, which again is insufficiently fine-scale to adequately resolve important
150 features such as foehn winds.

151

152 Some attempts have been made to link specific atmospheric drivers to increased melting over
153 the ice shelves on the eastern side of the Antarctic Peninsula using a variety of methods. For
154 instance, Cape et al. (2015) use satellite and Automatic Weather Station (AWS) data to
155 correlate monthly Antarctic Peninsula foehn occurrence with backscatter-derived surface
156 melt and find the strongest relationships on the Larsen A and B ice shelves and in inlets in the
157 northwest of Larsen C ice shelf. Kuipers Munneke et al. (2018) demonstrate that a foehn
158 event drove enhanced surface melting across Larsen C during austral autumn (March, April,
159 May; MAM) 2016. Elvidge et al. (2020) also find that foehn winds are the dominant
160 meteorological driver of melt across Larsen C, with the primary cause of melting attributed to
161 incoming shortwave (SW) radiation, a result also reported by Gilbert et al. (2020) for DJF
162 2011. Foehn events are commonly associated with leeside cloud clearance and thus enhanced
163 SW radiation (e.g., Takane and Kusaka 2011).

164

165 Gilbert et al. (2020) identify cloud phase as a crucial determinant of melting over Larsen C
166 because optically thick clouds with larger ice or liquid water paths (IWP or LWP) decrease
167 downward SW radiation and increase downward longwave (LW) radiation, and whether the
168 cloud enhances or suppresses melt depends on the balance between these radiative effects
169 (Hofer et al., 2019). Optically thick cloud is shown by Ghiz et al. (2021) to increase
170 downward LW fluxes enough to initiate and prolong periods of melting in West Antarctica,

171 while optically thin liquid-bearing cloud can also enhance melting by increasing the total
172 downward radiative flux, a phenomenon also noted in Greenland by Bennartz et al. (2013).
173 Although demonstrated for short periods (Gilbert et al., 2020), the importance of cloud-
174 mediated melting on Larsen C has not been examined over multiple decades.

175

176 Given these knowledge gaps, the aim of this investigation is to robustly quantify the
177 importance of the various drivers of Larsen C surface melting over a multi-decadal period.
178 This is critical for understanding Larsen C's stability in the context of past, present and future
179 change. For example, Trusel et al. (2015), Lai et al. (2020) and Gilbert & Kittel (2021)
180 identify Larsen C as being vulnerable to hydrofracturing-mediated collapse as the climate
181 warms. By bringing together the many atmospheric drivers or conditions that are
182 demonstrably important in the region, such as foehn, cloud phase and large-scale circulation
183 variability, this study will comprehensively determine their impact on the SEB and surface
184 melting over Larsen C-

185

186 We will do this by examining output from the high-resolution multi-decadal MetUM hindcast
187 of the Antarctic Peninsula described in Part 1 of this study (Gilbert et al., 2022), which
188 included a validation of the model SEB against AWS measurements on Larsen C. Part 1
189 showed that the hindcast is capable of representing the foehn-induced east-west gradient in
190 surface melting on Larsen C observed by satellites (Bevan et al., 2018), i.e., indicating that it
191 is able to reasonably represent foehn-associated flow. It further shows that the model captures
192 the observed frequency of foehn events over Larsen C, and adequately simulates near-surface
193 meteorology. This hindcast is therefore a useful resource for studying the dominant
194 conditions that influence surface melting on the Larsen C ice shelf.

195

196 **2 Data & Methods**

197

198 2.1 The surface energy balance and surface melt

199 The influence of atmospheric processes on surface melting is quantified by examining their
200 effect on the SEB, defined as the balance between upwelling and downwelling components
201 of surface SW and LW radiation, SW_{\uparrow} , SW_{\downarrow} , LW_{\uparrow} and LW_{\downarrow} respectively, and the latent,
202 sensible and ground heat fluxes, H_s , H_L and G_s , respectively, and which is formulated as:

203
$$E_{tot} = LW_{\uparrow} + LW_{\downarrow} + SW_{\uparrow} + SW_{\downarrow} + H_S + H_L + G_S \quad (1)$$

204 where fluxes directed towards the snow surface are defined as positive. Surface melt energy,
 205 E_{melt} , is positive when the sum of fluxes, E_{tot} , is positive and surface temperature, T_S , is at or
 206 above the melting point, i.e.:

207
$$E_{melt} = \begin{cases} E_{tot} & T_S \geq 0^{\circ}\text{C} \\ 0 & T_S < 0^{\circ}\text{C} \end{cases} \quad (2)$$

208

209

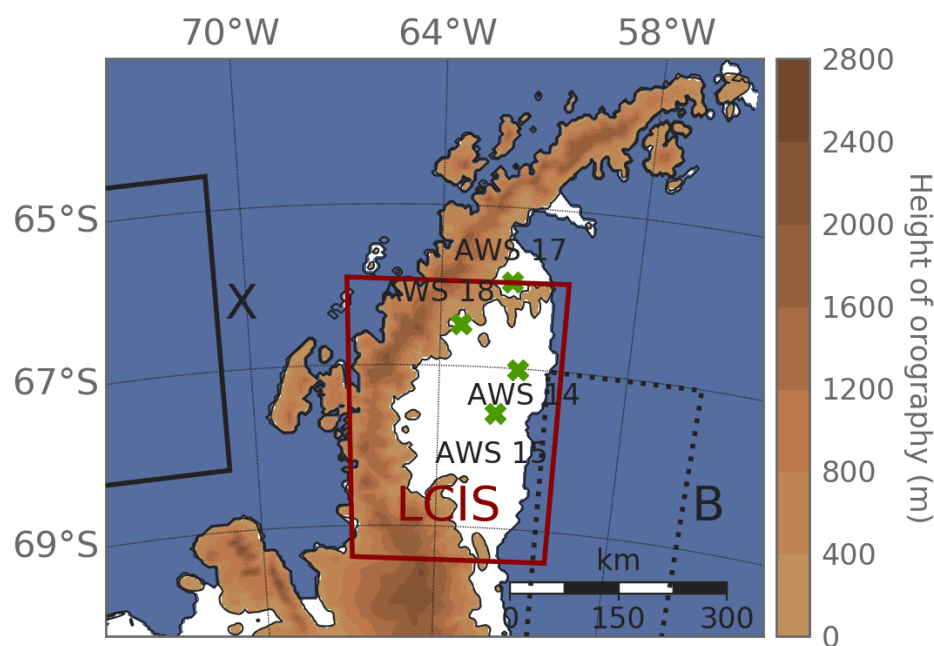
2.2 The MetUM model

210

211 As the MetUM hindcast is comprehensively described and evaluated in Gilbert et al. (2022),
 212 this section will only give brief details of the simulation. The hindcast uses a spatial
 213 resolution of 4 km over a domain that covers the central Antarctic Peninsula, centred on the
 214 Larsen C ice shelf (Figure 1). Boundary conditions are from ERA-Interim. It has output at
 215 three and six hourly temporal resolution for one/two-dimensional and three-dimensional
 216 variables, respectively. The variables archived include SEB terms (turbulent and radiative
 217 fluxes), near-surface meteorology (winds, humidity, temperatures, pressure etc.), cloud fields
 218 (water paths, mass mixing ratios, cloud fractions etc.) and surface melt terms as well as three
 219 dimensional winds, potential temperature, air temperature and specific humidity on model
 220 and pressure levels. A full description of the outputs can be found at Gilbert (2020a).

221

222 On average, Gilbert et al. (2022) found that the MetUM hindcast simulates conditions over
 223 Larsen C that are slightly warmer, windier and moister compared to observations from
 224 AWSs, and that net surface radiation, R_{net} , ($LW_{net} + SW_{net}$) and E_{melt} are under-estimated. The
 225 hindcast represents many components of the SEB well, for example model SW albedo is
 226 simulated to within 1% and 3% of observed values at inlet and ice shelf AWSs, respectively.
 227 Inlet stations are situated along the western edge of the ice shelf at the base of the Antarctic
 228 Peninsula, and ice shelf stations are situated over the homogeneous ice to the east of the
 229 Peninsula. Downwelling surface radiative fluxes are simulated within 10% of observed
 230 values at both inlet and ice shelf stations. However, even small compensating errors in the
 231 downwelling fluxes, for instance related to errors in the simulated cloud field, have
 232 implications for interpreting the results. Positive T_S and consequently LW_{\uparrow} biases result in
 233 negative R_{net} and E_{melt} biases that are more pronounced at inlet stations, and during DJF.
 234 More detailed validation can be found in Part 1.



235

236 **Figure 1.** Map of the Antarctic Peninsula MetUM hindcast model domain, with the locations
 237 of the four AWSs used for validation indicated with green crosses. The map is centred on the
 238 Larsen C ice shelf and its tributary inlets, and also shows the remnant Larsen B ice shelf on
 239 which AWS 17 is located. The mean modelled height of orography is indicated with coloured
 240 contours and is derived from the RAMP 200 m elevation model (Liu, 2015). The three
 241 regions used in the diagnosis of conditions influencing melt are also shown. Abbreviations
 242 used in the plot are as follows. "X": region in which u_{z1} is calculated, used for diagnosing
 243 foehn conditions; "B": region for diagnosing barrier wind conditions; "LCIS": Larsen C box
 244 used to calculate means for high and low melt, high and low LWP, sunny, cloudy and clear
 245 conditions.

246

247 2.3 Diagnosing dominant conditions

248 The relative importance of various drivers of surface melting is assessed by examining
 249 periods when certain conditions prevail, which have been identified from the literature
 250 summarised in section 1. These include: sunny, foehn, cloudy, clear, high/low LWP, barrier
 251 wind, ASL, positive/negative SAM, positive/negative ENSO, and high/low melt conditions.
 252 These are listed in Table 1 and defined in full below. Large-scale circulation patterns (i.e.,
 253 SAM, ASL and ENSO) are diagnosed using observed indices. All other conditions are
 254 determined from model output and diagnosed from "indicator variables", which are the
 255 parameters that reveal whether or not certain conditions prevail. The regions used for

256 averaging indicator variables are shown in Figure 1 and data sources and treatments are
 257 described in detail in Table 1.

258

259 **Table 1.** Indicator variables, thresholds and regions used in diagnosing the conditions used
 260 for compositing. Prevailing conditions are abbreviated as defined in the main text, where the
 261 acronyms "SAM", "ENSO" and "ASL" refer to the Southern Annular Mode, El Niño
 262 Southern Oscillation and Amundsen Sea Low, respectively. The regions used are indicated in
 263 Figure 1. Note that high and low melt conditions are responses to forcing (such as foehn
 264 conditions or SW radiation) rather than causes of melting themselves and are used to guide
 265 the analysis in section 3.

Condition	Indicator variable	Threshold	Region
Low melt	Meltwater production	< 25 th percentile	Region "LCIS"
High melt	Meltwater production	> 75 th percentile	Region "LCIS"
Sunny	SW _↓	> 75 th percentile	Region "LCIS"
Barrier wind	V wind	5.0 m s ⁻¹	Region "B"
Foehn	U wind, T _{air} , RH, potential temperature	≥ 6 3-hour periods of foehn at 3 AWSs (see main text for details).	u _{Z1} calculated in region "X", T _{air} and RH changes calculated in the grid box of interest
ASL	Hosking et al. (2013) index	Pressure anomaly below 25 th percentile	Pressure centre north of 70°S
SAM+	SAM index	+1 σ (+1.36)	N/A
SAM-	SAM index	-1 σ (-1.36)	N/A
ENSO+ (La Niña conditions)	Nino3.4 index	+0.5	N/A
ENSO- (El Niño conditions)	Nino3.4 index	-0.5	N/A

266

267

268 Foehn conditions are diagnosed when foehn winds are detected in the model data for at least
269 six 3-hour periods in a day at the locations of all of the three AWSs on the Larsen C ice shelf
270 (AWS 14, 15 and 18; See Figure 1 for their location), which may indicate either foehn
271 conditions occurring persistently at one AWS (i.e. for 18+ hours in a day) or foehn occurring
272 at all three AWSs (i.e. for 6+ hours in a day), or a combination of these situations. Foehn
273 events at each AWS location are detected using the isentrope-based method described in
274 Gilbert et al. (2022), which diagnoses foehn conditions over Larsen C if the following occur:
275 a) the mean upstream zonal flow impinging on the Antarctic Peninsula between
276 approximately 250-2500m altitude, u_{z1} , has a clear westerly component (i.e., $u_{z1} \geq 2 \text{ m s}^{-1}$)
277 so that the oncoming flow can be forced over the Peninsula (Orr et al., 2008; 2021), b) the
278 upwind isentrope at altitude Z1 (~2500 m) falls downstream of the Peninsula (over Larsen C)
279 by an altitude of at least 500 m over a 6-hour period, and c) warming of the atmospheric
280 column is simulated over Larsen C, resulting in warming and drying at the ice shelf surface.

281

282 Sunny conditions are diagnosed when the mean incoming solar radiative flux (SW_{\downarrow}) over the
283 Larsen C ice shelf (averaged over the region marked “LCIS” in Figure 1) exceeds the 75th
284 percentile of 20-year mean SW_{\downarrow} for the day of the year considered. SW_{\downarrow} is therefore the
285 “indicator variable” that enables the detection of these conditions. Cloudy and clear
286 conditions are detected using cloud fraction, averaged over the “LCIS” region in Figure 1,
287 according to the thresholds of Kay et al. (2008). “Cloudy” conditions are diagnosed when the
288 mean cloud fraction exceeds 0.75, while “clear” conditions occur when cloud fraction is
289 below 0.31. High and low LWP conditions occur when the mean LWP over the “LCIS”
290 region falls above and below the 75th and 25th percentiles for that day of the year,
291 respectively, in a manner similar to the diagnosis of sunny conditions. High and low IWP
292 conditions are not examined because liquid cloud was shown to exert a more important
293 control on the SEB and surface melting over Larsen C in Gilbert et al. (2020).

294

295 Barrier wind conditions are diagnosed when mean 10 m meridional wind speeds in the
296 Weddell Sea region (marked “B” in Figure 1 **Error! Reference source not found.**) exceed 5
297 m s^{-1} , indicative of strong near-surface southerly flow. Modelled 20-year mean meridional
298 wind speeds in this region are 1.13 m s^{-1} , so this threshold represents a significant increase.
299 High and low melt periods are determined using the 75th and 25th percentiles of meltwater
300 production, respectively, averaged over the “LCIS” region.

301

302 The daily mean SAM index is that of the US National Oceanic and Atmospheric
303 Administration (NOAA)'s National Weather Service Climate Prediction Centre and is
304 calculated from National Center for Environmental Prediction/National Center for
305 Atmospheric Research reanalysis at $2.5^\circ \times 2.5^\circ$ resolution (CCP, 2005). Positive and negative
306 SAM periods are abbreviated as "SAM+" and "SAM-", respectively. The Niño3.4 dataset
307 (Reynolds et al., 2007), which is used by the World Meteorological Organisation and NOAA
308 to diagnose El Niño and La Niña events, is used to diagnose the phase of ENSO at daily
309 frequency. El Niño and La Niña periods are abbreviated to "ENSO-" and "ENSO+",
310 respectively. Positive and negative phases of these circulation modes are detected when the
311 index is above/below plus/minus one standard deviation of the time series 1998-2017.
312 Positive and negative ENSO periods are diagnosed when three-month running mean
313 anomalies are above or below 0.5°C or -0.5°C , respectively, according to the method of
314 NOAA (see <https://www.weather.gov/fwd/indices>, accessed 30/06/2020).

315

316 The influence of the ASL is examined using the observed index of Hosking et al. (2013),
317 which measures the depth and longitude of the ASL. Deep ASL conditions (hereafter referred
318 to simply as 'ASL conditions') are diagnosed when the relative central pressure is less than
319 the 25th percentile and its latitude is north of 70°S , where it will have a more notable impact
320 on conditions over Larsen C. (Here the relative central pressure is defined by subtracting the
321 actual central pressure from an area-averaged pressure over the ASL sector, defined as 170° -
322 298° E, 80° - 60° S, see Hosking et al., 2013).

323

324 2.4 Analysis methods

325

326 The study employs two primary analysis methods. Firstly, Pearson correlation coefficients (r
327 values) between pertinent variables (such as E_{melt} and SW_l) are examined to quantify the
328 strength of the relationships between modelled variables. The statistical significance of the
329 relationship is also calculated as a two-sided p value. Secondly, a composite approach is
330 used, in a similar manner to Deb et al. (2018). During periods when particular conditions are
331 diagnosed as described above, mean meteorological variables (3-hourly mean 10 m winds,
332 1.5 m air temperature and MSLP) and SEB parameters (SW , LW , H_s , H_L , E_{tot} and E_{melt}) are
333 averaged to produce a composite that represents the meteorological state during these
334 conditions. The relative proportion of total melt produced during conditions characteristic of
335 each melt driver, as well as the proportion of time in which those conditions occur, were also

336 calculated in order to quantify the importance of each driver of surface melt on Larsen C. All
337 analysis was performed seasonally and is based on model output for the 1998-2017 period.

338

339

340 **3 Results & Discussion**

341

342 The drivers of surface melting are first considered by examining the “high melt” composites.
343 After this, we assess the role of the most important controls on surface melt.

344

345 3.1 “High melt” composites

346 Figure 2 shows composited mean seasonal conditions during high melt conditions (melt
347 amount > 75th percentile, Table 2); panels a-c show daily near-surface meteorological
348 conditions, while daily E_{melt} anomalies relative to the climatology for 1998-2017 are shown
349 in panels d-f. Figure 2 shows that for all seasons, instances of high melting over Larsen C
350 occur during periods of north-westerly flow, which produces cross-peninsula winds and
351 therefore is conducive to establishing foehn conditions, and/or the advection of relatively
352 warm and moist maritime air across the Antarctic Peninsula.

353

354 Consistent with Kuipers Munneke et al. (2018) and Elvidge et al. (2020), these conditions are
355 associated with significant increases in H_s (not shown), and consequently in E_{tot} and E_{melt}
356 over Larsen C, driving surface melting particularly during DJF when surface temperature is
357 higher. During DJF high melt conditions are associated with high SW_{\downarrow} fluxes, causing
358 temperatures to be at the melt point more frequently. Compared to the other seasons, DJF is
359 also associated with comparatively weaker cross-peninsula flow and comparatively small
360 T_{max} anomalies (Figure 2b). Around 63% of DJF meltwater production over Larsen C occurs
361 in high melt periods (Table 2), which take place over the entire ice shelf (Figure 2e). This
362 differs from SON, MAM and JJA, when melting occurs almost exclusively during intense
363 melt events (Kuipers Munneke et al., 2018) associated with cross-peninsula flow and is
364 confined to the western regions of the ice shelf (Figure 2d,f, JJA not shown), with 93%, 98%
365 and 97% of seasonal meltwater production occurring in just 9%, 7% and <1% of the time,
366 respectively (Table 2).

367

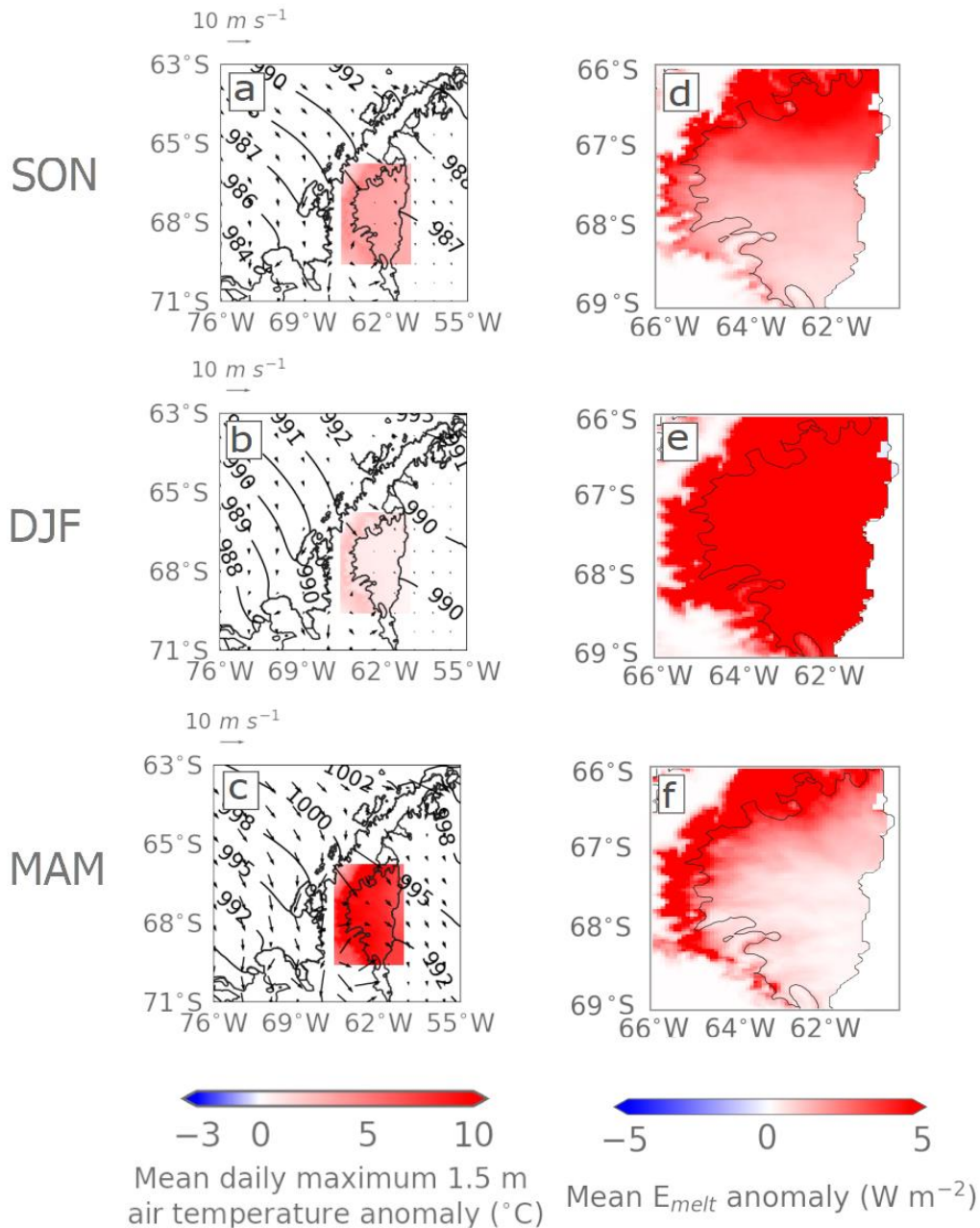
368 The following sub-sections examine in turn the role of each of the various conditions
369 described in Section 2.3 on surface melt over Larsen C.

370 **Table 2.** Percentage of total modelled meltwater production (%) associated with the
 371 conditions evaluated during each season for the hindcast period, and the frequency at which
 372 they occur (%).

	DJF		MAM		JJA		SON	
	Melt amount	Frequency	Melt amount	Frequency	Melt amount	Frequency	Melt amount	Frequency
Low melt	0.8	24.5	0.0	7.1	0.1	0.6	0.1	9.1
High melt	63.0	24.5	97.6	7.2	96.7	0.7	92.5	9.1
Sunny	41.7	25.0	47.1	25.0	0.3	25.0	75.2	25.0
Foehn	22.4	18.7	54.8	16.7	97.3	20.9	47.6	23.7
Cloudy	50.2	61.6	69.1	54.6	95.5	56.9	56.6	61.7
Clear	9.8	7.8	2.4	9.2	0.0	10.8	4.2	6.9
Low LWP	32.0	25.0	4.2	25.0	0.0	25.0	8.4	25.0
High LWP	15.2	25.0	44.4	25.0	90.7	25.0	35.7	25.0
SAM+	25.0	21.9	38.9	17.3	21.9	22.2	24.5	16.9
SAM-	8.5	9.3	0.5	10.7	0.1	15.6	10.9	16.4
ENSO+	38.1	40.0	17.1	35.5	1.5	15.3	34.7	27.3
ENSO-	34.6	33.5	65.6	23.2	3.8	15.2	29.5	28.1
ASL	6.4	3.3	19.9	11.7	0.2	11.6	19.4	36.6
Barrier	3.8	10.8	0.0	15.9	0.0	19.2	1.4	18.3

373

374



375
 376 **Figure 2.** Compositing daily mean conditions during "high melt" conditions (melt amount >
 377 75th percentile) for spring (SON), summer (DJF), and autumn (MAM), for the hindcast
 378 period. JJA is not shown because the amount of melting occurring during winter is negligible.
 379 Panels a) to c) show mean synoptic meteorological conditions, where coloured shading shows
 380 the daily maximum 1.5 m air temperature anomaly (T_{max} ; units $^{\circ}\text{C}$), and contours and vectors
 381 give mean sea level pressure (hPa) and 10 m wind speed and direction, respectively. Panels
 382 d) to f) show anomalies in surface melt (E_{melt} ; units W m^{-2}). Anomalies are computed relative
 383 to the 1998-2017 model climatology. Synoptic meteorology plots show the wider Antarctic
 384 Peninsula region, while the E_{melt} plots focus on the Larsen C ice shelf.

385

386 3.2 Drivers of modelled surface meltwater production

387 3.2.1 Solar radiation

388 Table 3 shows Pearson correlation coefficients between daily E_{melt} and other SEB
389 components over the Larsen C ice shelf for the entire hindcast period. The largest annual
390 correlation between E_{melt} and the fluxes in Table 3 is with net SW radiation, SW_{net} ($r_{SW_{net},melt} =$
391 0.56). This relationship is also seen in DJF ($r_{SW_{net},melt} = 0.45$), which supports the findings of
392 Gilbert et al. (2020) that SW radiation is a dominant driver of summertime surface melting.
393 90% of hindcast-simulated surface melting occurs in DJF (not shown) when SW_{\downarrow} is highest,
394 which suggests that meltwater production is driven predominantly by SW_{\downarrow} . This result is
395 consistent with Elvidge et al. (2020) and Gilbert (2020b), who also find that SW radiation is
396 the dominant cause of surface melting during summer. Correlations are insignificant in JJA
397 (Table 3) when there is very little SW_{\downarrow} and <0.1 % of meltwater production occurs. For this
398 reason, JJA is not included in Figure 2 or subsequent composite figures.

399

400 **Table 3.** Pearson correlation coefficients (r) between E_{melt} and SW_{\downarrow} , SW_{net} , LW_{\downarrow} , LW_{net} , H_s ,
401 and H_L over the Larsen C ice shelf during each season, and annually, for the hindcast period.
402 Only values that are significant at the 99% level are shown.

	DJF	MAM	JJA	SON	ANN
SW_{\downarrow}	0.42	-	-	0.29	0.52
SW_{net}	0.45	-	-	0.33	0.56
LW_{\downarrow}	-	0.15	-	0.22	0.33
LW_{net}	-0.19	-	-	-	-0.12
H_s	0.38	0.28	0.11	-	-
H_L	0.15	0.08	-	-0.14	-0.19

403

404

405 Table 2 shows that ‘sunny’ conditions ($SW_{\downarrow} > 75^{th}$ percentile) occur 25% of the time in DJF,
406 yet account for 42% of total DJF meltwater production (and around 38% of the annual total,
407 not shown in Table 2). The proportion of meltwater production associated with ‘sunny’
408 conditions increases to 47% and 75% in MAM and SON, respectively (Table 2), indicating
409 that periods of above-average insolation are important for driving surface melt during these
410 seasons, particularly during SON. Once the frequency of occurrence is accounted for, ‘sunny’

411 conditions account for the highest percentage of meltwater production of any driver in DJF
412 and SON. This is also apparent from Figure 3, which shows that the largest DJF E_{melt}
413 anomalies are associated with ‘sunny’ conditions. ‘Sunny’ conditions are associated with
414 extensive positive E_{melt} anomalies across the ice shelf, especially during DJF (Figure 3m) but
415 also during SON (Figure 3j), partly because extensive T_{max} anomalies occur during such
416 periods, especially in DJF (Figure 3d).

417

418 The co-occurrence of ‘high melt’ and ‘sunny’ conditions can also be used to demonstrate the
419 importance of SW radiation in driving more intense melt events. During SON, DJF and
420 MAM, ‘high melt’ and ‘sunny’ conditions co-occur 73%, 50% and 46% of the time,
421 respectively (not shown). The high co-occurrence during SON suggests that SW radiation is
422 especially important for driving the most intense melt events, whereas high melt periods in
423 DJF when SW_{\downarrow} is more similar to climatological conditions can still account for a
424 comparatively large amount of melting. Because 96% of total annual melt occurs during
425 these two seasons, these results suggest that SW radiation is the most important driver of
426 surface melting on Larsen C overall.

427

428 3.2.2 Foehn

429

430 The frequency of foehn events at inlet and ice shelf stations is diagnosed using the isentrope-
431 based method described in section 2.3 and composites of near-surface meteorology and
432 surface fluxes when foehn winds are detected are shown in the second column of Figure 3.
433 Foehn conditions are associated with strong north-westerly flow and positive T_{max} anomalies
434 in all seasons (Figures 3b, e, h), which has different effects on E_{melt} in different seasons
435 (Figures 3k, n, q). During JJA (not shown), temperatures are largely too low for melting to
436 occur. In contrast, in DJF foehn events are associated with positive E_{melt} anomalies that are
437 distributed fairly evenly across Larsen C (Figure 3n), with slightly higher anomalies in inlets
438 below the peaks in orography, i.e., there is a zonal gradient in melt. E_{melt} anomalies in SON
439 (Figure 3k) are similarly extensive, but of lower magnitude, whereas much more intense,
440 confined melting is simulated in the immediate lee of steep topography in MAM (Figure 3q).

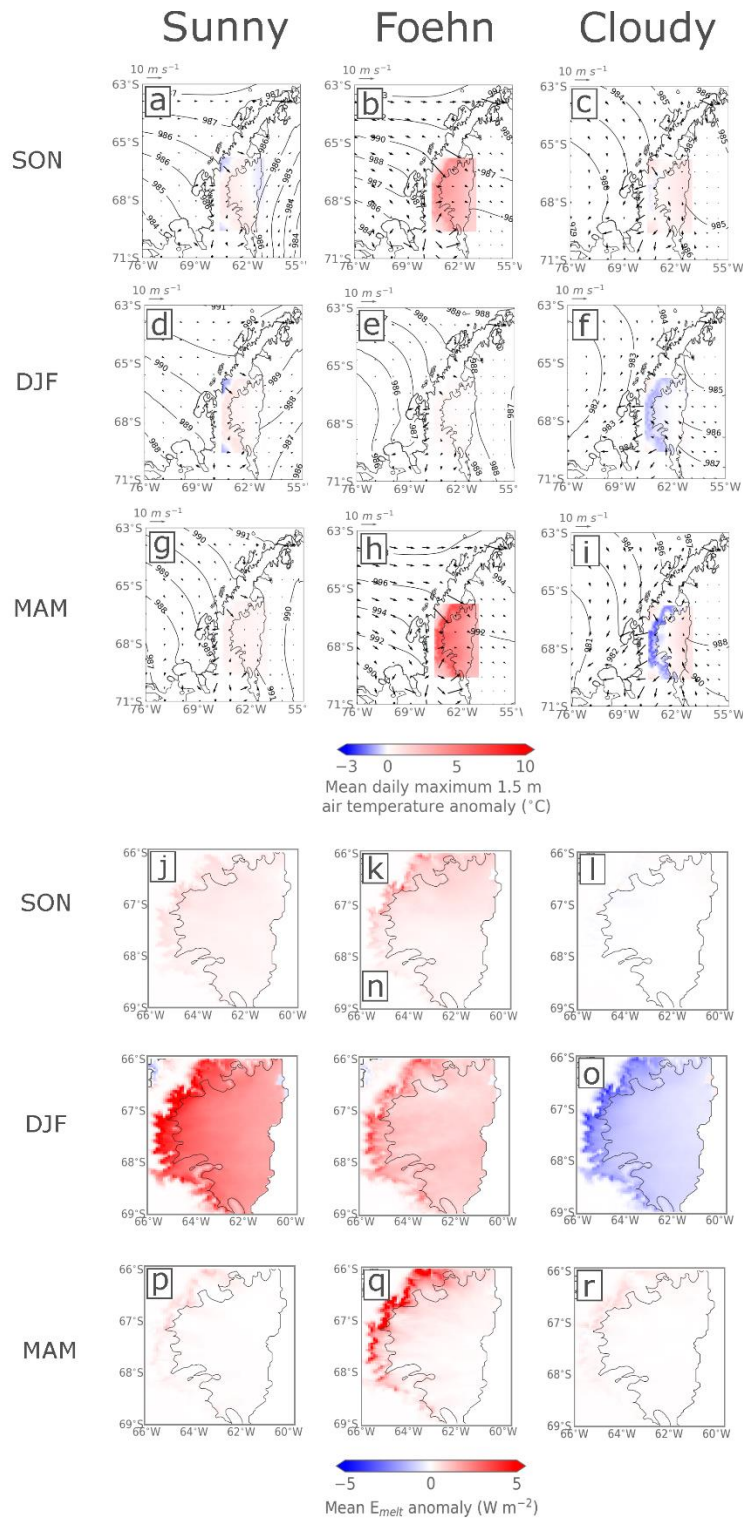
441

442 Using the isentrope-based method, foehn conditions are diagnosed 92%, 49%, 40% and 24%
443 of the time that ‘high melt’ conditions shown in Figure 2 also occur in JJA, MAM, SON and
444 DJF, respectively (not shown). Foehn are less important for driving intense melt events in

445 DJF because foehn occur less frequently (19% of the time, Table 2) and have less impact
446 (accounting for 22% of melt, Table 2) because SW radiation is the primary driver of melting
447 in summer and temperatures are already closer to the melting point. This is evident in Figure
448 3 from the lower T_{\max} anomalies associated with foehn conditions in DJF (panels b, e, h). As
449 shown in section 3.2.1, SW radiation is the most important driver of intense melt events in
450 SON (Figure 3j), although the foehn conditions are still associated with 48% of SON melt
451 despite occurring only 24% of the time (Table 2). During MAM, foehn is far more important
452 than SW, with ‘foehn’ conditions associated with 55% of MAM melting, despite occurring
453 just 17% of the time (Table 2). This is also apparent from Figures 3 (panels p and q) and 4.
454

455 The above results show that foehn events are an important driver of surface melting over the
456 Larsen C ice shelf year-round but are especially important in non-summer seasons. As
457 discussed earlier, foehn events are associated with positive H_S fluxes because they bring
458 warm air to the surface. Accordingly, positive correlations are simulated between E_{melt} and
459 H_S in DJF, JJA and MAM (Table 3), although these are larger during DJF and MAM. This
460 result is consistent with Elvidge et al. (2020), who find that regimes dominated by large
461 positive H_S fluxes account for a large amount of melting in non-summer seasons, and that
462 76% of melting during foehn conditions occurred when H_S fluxes were large. The combined
463 effect of foehn and warmer air temperatures may explain why the correlation between E_{melt}
464 and H_S is higher in the warmer seasons of DJF and MAM (Table 3). The negative correlation
465 between E_{melt} and H_L during SON and ANN ($r_{H_L, \text{melt}} = -0.14$ and -0.19 , respectively, Table 3)
466 suggests that melting in these seasons primarily occurs when air is anomalously warm and
467 dry, driving upward (i.e., negative) H_L fluxes, consistent with foehn conditions. The weak
468 correlation coefficients given in Table 3 between E_{melt} and the turbulent heat fluxes, which
469 are themselves only a proxy for foehn events, cannot conclusively demonstrate the
470 importance of foehn in driving surface melting. However, they add weight to the evidence
471 presented above.

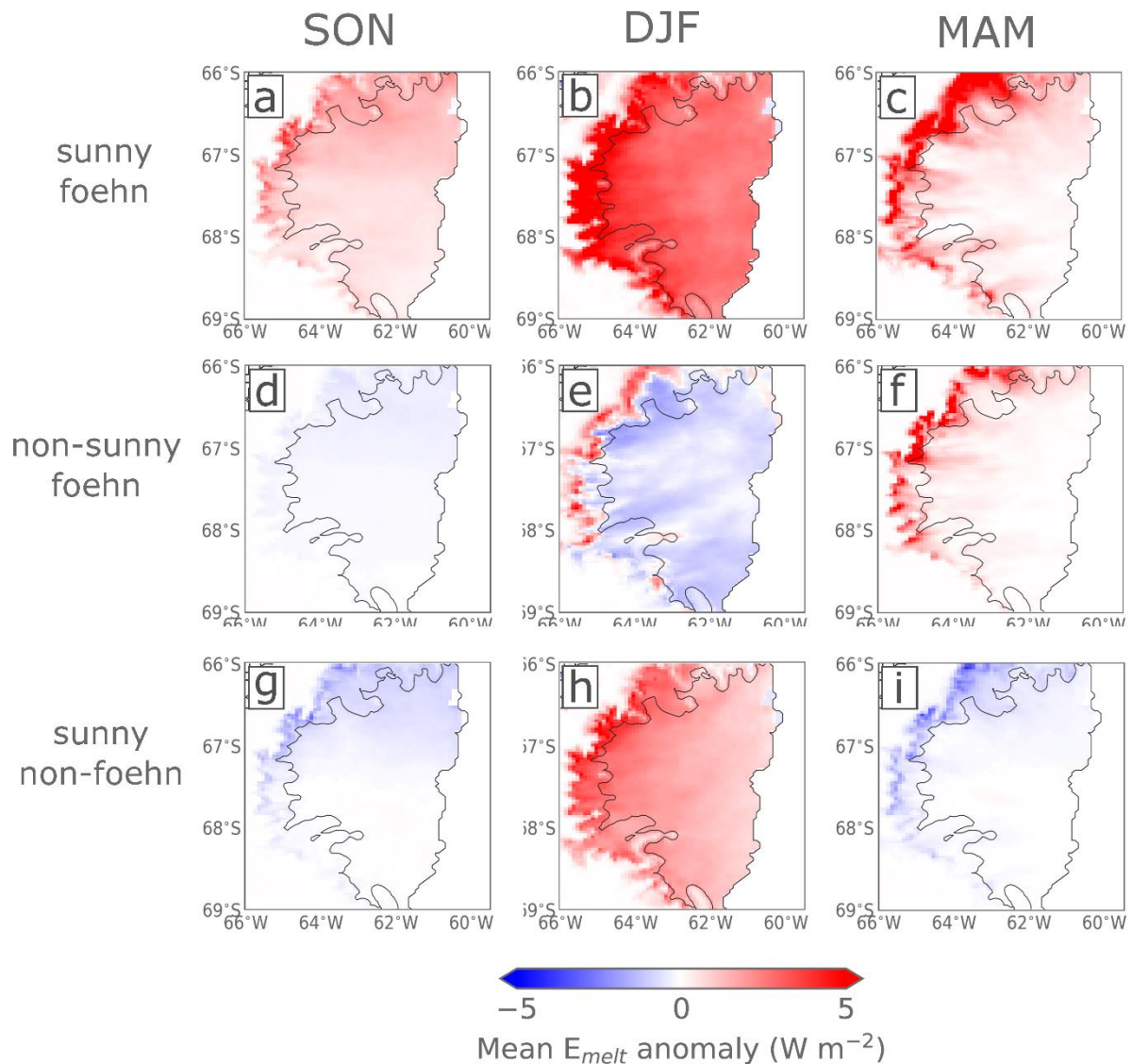
472
473
474



475

476 **Figure 3.** As in Figure 2 but showing composited mean synoptic near-surface meteorology
 477 (panels a-i) and E_{melt} fluxes (panels j-r) in ‘sunny’ (first column), ‘foehn’ (second column)
 478 and ‘cloudy’ (third column) conditions during SON (first and fourth rows), DJF (second and
 479 fifth rows) and MAM (third and sixth rows) for the hindcast period. JJA is not shown because
 480 $<0.1\%$ of melting occurs during winter. Contours, vectors, colours and shading are as in
 481 Figure 2.

482 Figure 4 shows mean E_{melt} anomalies in seasons SON, DJF, and MAM for ‘sunny foehn’,
483 ‘non-sunny foehn’ and ‘sunny non-foehn’ conditions, which allows us to further elucidate the
484 relative importance of SW and foehn on melting over Larsen C. In all seasons, ‘sunny foehn’
485 conditions account for more positive E_{melt} anomalies than either ‘sunny’ or ‘foehn’ conditions
486 alone (e.g., compare Figure 3j, m, p and 3k, n, q with Figure 4a-c). In DJF, foehn conditions
487 slightly enhance melting in inlets (Figure 3n), but SW radiation is evidently much more
488 important for driving melt across the ice shelf because when SW_{\downarrow} is low, foehn conditions are
489 associated with negative E_{melt} anomalies across much of Larsen C (Figure 4e). However, in
490 MAM the opposite is true, suggesting that foehn conditions are a more important driver of
491 melt in this season than SW radiation: even when $SW_{\downarrow} > 75^{\text{th}}$ percentile, if foehn conditions
492 are not also simulated, E_{melt} anomalies are negative (Figure 4i). In SON, both foehn and
493 sunny conditions must be simulated to generate positive E_{melt} anomalies. E_{melt} anomalies are
494 negative during ‘non-sunny foehn’ and ‘sunny non-foehn’ conditions (Figure 4d and 4g), but
495 positive in ‘sunny foehn’ (Figure 4a), which is consistent with the small positive E_{melt}
496 anomalies associated with both ‘foehn’ and ‘sunny’ shown in Figure 3j and 3k.
497



498

499 **Figure 4.** As in Figure 2, but showing seasonal E_{melt} anomalies only for SON (first column),
 500 DJF (second column) and MAM (third column) during three separate conditions for the
 501 hindcast period: ‘sunny foehn’ when $SW_{\downarrow} > 75^{\text{th}}$ percentile *and* foehn conditions are
 502 simulated (panels a-c); ‘non-sunny foehn’ when foehn conditions are simulated but $SW_{\downarrow} <$
 503 25^{th} percentile (panels d-f); and ‘sunny non-foehn’ when $SW_{\downarrow} > 75^{\text{th}}$ percentile is simulated
 504 but foehn conditions are not (panels g-i).

505

506 3.2.3 Cloud

507 To examine the role of cloud on surface melting, composites of ‘cloudy’ conditions are
 508 shown in the third column of Figure 3. During DJF, cloudy conditions are associated with an
 509 easterly flow of maritime air from the Weddell Sea and negative T_{max} anomalies on Larsen C
 510 (Figure 3f). This part of the Weddell Sea is typically ice-free during summer, so relatively

511 warm, moist maritime air is advected over the cold ice shelf, resulting in cooling of the air
512 and condensation. Further examination of the hindcast output shows that enhanced LW_{\downarrow}
513 produces positive E_{tot} anomalies and a mean absolute value of 9.3 W m^{-2} over ice shelf areas
514 away from the inlets, but because temperatures typically do not reach the melting point
515 during cloudy periods (mean T_{max} during ‘cloudy’ conditions is around -1.1°C), and because
516 SW_{\downarrow} is reduced, melt anomalies are negative (Figure 3o). Therefore, despite occurring 62%
517 of the time in DJF, ‘cloudy’ conditions are associated with just 50% of melt (Table 2). SON
518 composites (Figure 3c and 3l) mirror the DJF composites, with cloudy conditions suppressing
519 melt relative to the climatology. Cloudy conditions occur 62% of the time in SON but are
520 associated with just 57% of melt (Table 2).

521

522 During JJA, cloudy conditions, generated by cyclonic flow to the east and southerly winds
523 over Larsen C, are associated with positive T_{max} anomalies (not shown). Table 2 shows that
524 E_{melt} anomalies in JJA are almost zero because melt occurs so infrequently in JJA, but 95% of
525 the melting that does occur is associated with cloudy conditions (91% for high LWP, Table
526 2). Cloudy composites during MAM (Figure 3i and 3r) are comparable to those during JJA,
527 with cloud enhancing E_{melt} : 69% of MAM melting occurs in cloudy periods, which occur
528 55% of the time (Table 2).

529

530 Cloudy and clear conditions are typified by high and low liquid water path ($LWP > 75^{\text{th}}$
531 percentile and $< 25^{\text{th}}$ percentile), respectively, and synoptic conditions and SEB anomalies
532 during ‘cloudy’ conditions are virtually indistinguishable from those during the ‘high LWP’
533 regime (not shown), suggesting the prevalence of liquid-bearing cloud in the hindcast and its
534 importance in determining melt. To avoid repetition, we do not include figures showing high
535 LWP conditions because they are so similar.

536

537 The seasonal pattern outlined above is consistent with the correlation coefficients shown in
538 Table 2, which show that E_{melt} is positively correlated with LW_{\downarrow} in MAM, SON and annually
539 ($r_{LW_{\downarrow}, \text{melt}} = 0.15, 0.22$ and 0.33 , respectively). This supports the notion that LW_{\downarrow} is an
540 important cloud-mediated control on surface melting, as demonstrated by e.g. Zhang et al.
541 (1996) and Gilbert et al. (2020). Cloudy, high LWP conditions may also induce a ‘thermal
542 blanketing’ effect, whereby SW_{\downarrow} is attenuated and LW_{\downarrow} enhanced so that R_{net} is close to zero
543 or just positive. In these conditions, if H_s and surface temperatures are above zero, melting
544 can result (Ghiz et al., 2021).

545

546 Because mean daily T_{\max} during cloudy, high LWP conditions is only slightly below the
547 melting point (as noted above) and the large LW_{\downarrow} fluxes associated with cloud produce
548 positive E_{tot} fluxes, this implies that cloud could become an important driver of surface melt
549 in a warming climate. Surface air temperatures on the eastern Antarctic Peninsula are
550 projected to warm by $\sim 0.5\text{-}3^{\circ}\text{C}$ by 2100 and could warm considerably more even under 1.5°C
551 global mean temperature rise (van Oldenborgh et al., 2013; Siegert et al., 2019), which would
552 mean the melting point could be reached more frequently in DJF during cloudy periods. This
553 could allow extensive low cloud-mediated melt events to occur such as were observed in
554 Greenland in 2012 (Bennartz et al., 2013) and which have been documented in West
555 Antarctica (Ghiz et al., 2021). As shown in Gilbert et al. (2020), cloud initiates summertime
556 melt by raising surface temperatures and producing an energy surplus (positive E_{tot}), which
557 then persists as cloud glaciation occurs and SW fluxes increase. This can induce a positive
558 feedback if melt occurs in sufficient volume to reduce the surface albedo, because the darker
559 melting surface can then absorb more SW radiation and sustain further melting. Because low-
560 level (liquid) cloud is typically extensive on Larsen C, this melting could occur across the
561 entire ice shelf.

562

563 3.2.4 Foehn-induced cloud clearance on Larsen C

564 The various combinations of ‘sunny’, ‘clear’, ‘LWP25’ and ‘foehn’ conditions can also be
565 used to examine the importance of cloud clearance on Larsen C, whereby warm, dry foehn air
566 reduces cloud cover and enhances melting by increasing SW_{\downarrow} (Hoinka et al., 1985). While
567 this mechanism has been proposed to explain enhanced melting over the ice shelf, e.g. by
568 Kuipers Munneke et al. (2012); Grosvenor et al. (2014); Cape et al. (2015); King et al. (2017)
569 and Elvidge et al. (2020), its significance has not yet been established across larger spatial
570 and temporal scales on Larsen C.

571

572 Foehn clearance can be defined as clear, sunny foehn periods with low LWP, or the
573 coincidence of foehn conditions with any of these criteria. Because model cloud fraction is
574 parameterised according to sub-grid scale variability in moisture, it can be less reliable than
575 prognostic diagnostics like LWP or solar radiation, so the definition is not necessarily as
576 straightforward as the coincidence of clear and foehn periods. Of the times when foehn
577 conditions are detected, ‘sunny’ conditions also occur 27%, 29% and 31% of the time in
578 MAM, SON and DJF, respectively (Table S1). Because cloudy conditions are so common on

579 Larsen C (occurring 55-62% of the time, as shown in Table 2), ‘cloudy foehn’ conditions also
 580 occur frequently, accounting for 35-59% of foehn periods depending on the season. ‘Clear
 581 foehn’ occur on average approximately five times less frequently (9-13% of foehn periods,
 582 Table S1). ‘Low LWP foehn’, which may include foehn periods where optically thin liquid
 583 clouds or high-level ice clouds are present, account for 25-31% of foehn periods and 12-20%
 584 of foehn periods are ‘high LWP foehn’ (Table S1).

585
 586

587 **Table 4.** Co-occurrence of ‘sunny’, ‘cloudy’, ‘clear’, ‘high LWP’, ‘low LWP’ and ‘foehn’
 588 conditions with ‘high melt’ conditions during each season. The values shown represent the
 589 percentage of time during which the conditions overlap with high melt conditions, that is, of
 590 the times that high melt conditions are occurring, what percentage of the time the conditions
 591 in question also occur.

	DJF	MAM	JJA	SON
Sunny	49.9%	45.5%	0.0%	73.3%
Foehn	23.7%	48.5%	92.3%	40.6%
Cloudy	44.2%	50.8%	84.6%	54.5%
Clear	9.7%	5.3%	0.0%	6.1%
High LWP	9.9%	34.1%	69.2%	40.0%
Low LWP	35.2%	8.3%	0.0%	8.5%
Sunny foehn (sunny + foehn)	12.9%	18.2%	0.0%	27.9%
Clear foehn (clear + foehn)	3.4%	3.0%	0.0%	4.8%
Cloudy foehn (cloudy + foehn)	10.6%	20.5%	76.9%	20.6%
Low LWP foehn (LWP25 + foehn)	9.3%	6.1%	0.0%	3.6%
High LWP foehn (LWP75 + foehn)	2.0%	10.6%	61.5%	12.1%

592

593 Table 4 shows how frequently high melt periods coincide with these conditions. Figure 5
 594 summarises the dominant combinations of conditions that occur during ‘high melt’ conditions
 595 in different seasons, and can be thought of as illustrating some of the primary ‘modes’ of
 596 melting over Larsen C. Sunny conditions co-occur with 46-73% of high melt periods
 597 (excluding JJA when SW radiation is negligible; Figure 5a, g), while foehn and cloudy
 598 conditions co-occur with 24-92% and 44-85% of high melt periods, respectively (Table 4,
 599 Figure 5c, f). Clear and high melt conditions co-occur relatively infrequently, coinciding for

600 <10% of the time high melt periods are detected in all seasons, consistent with clear
601 conditions occurring infrequently (7-11% of the time in Table 2). Similarly, in non-summer
602 seasons low LWP periods coincide quite rarely with high melt periods (8% in MAM and 9%
603 in SON, Table 4). In comparison, cloudy/high LWP conditions coincide with a much larger
604 percentage of high melt periods than clear/low LWP conditions (Table 4, Figure 5e). In DJF
605 however, while cloudy conditions coincide with a large proportion (44%) of high melt
606 periods, high LWP conditions do not. Instead, low LWP and high melt conditions more
607 commonly co-occur (35%). The importance of cloudy *and* low LWP conditions suggests that
608 optically thin, low-level clouds could be important for driving surface melting over Larsen C
609 during summer, as seen in Greenland and West Antarctica (Bennartz et al., 2013; Ghiz et al.,
610 2021, Figure 5b), or that cloud clearance at lower levels could drive melting while high-level
611 ice cloud is present (therefore resulting in a large cloud fraction, Figure 5c). The latter would
612 constitute cloud clearance but further investigation is required.

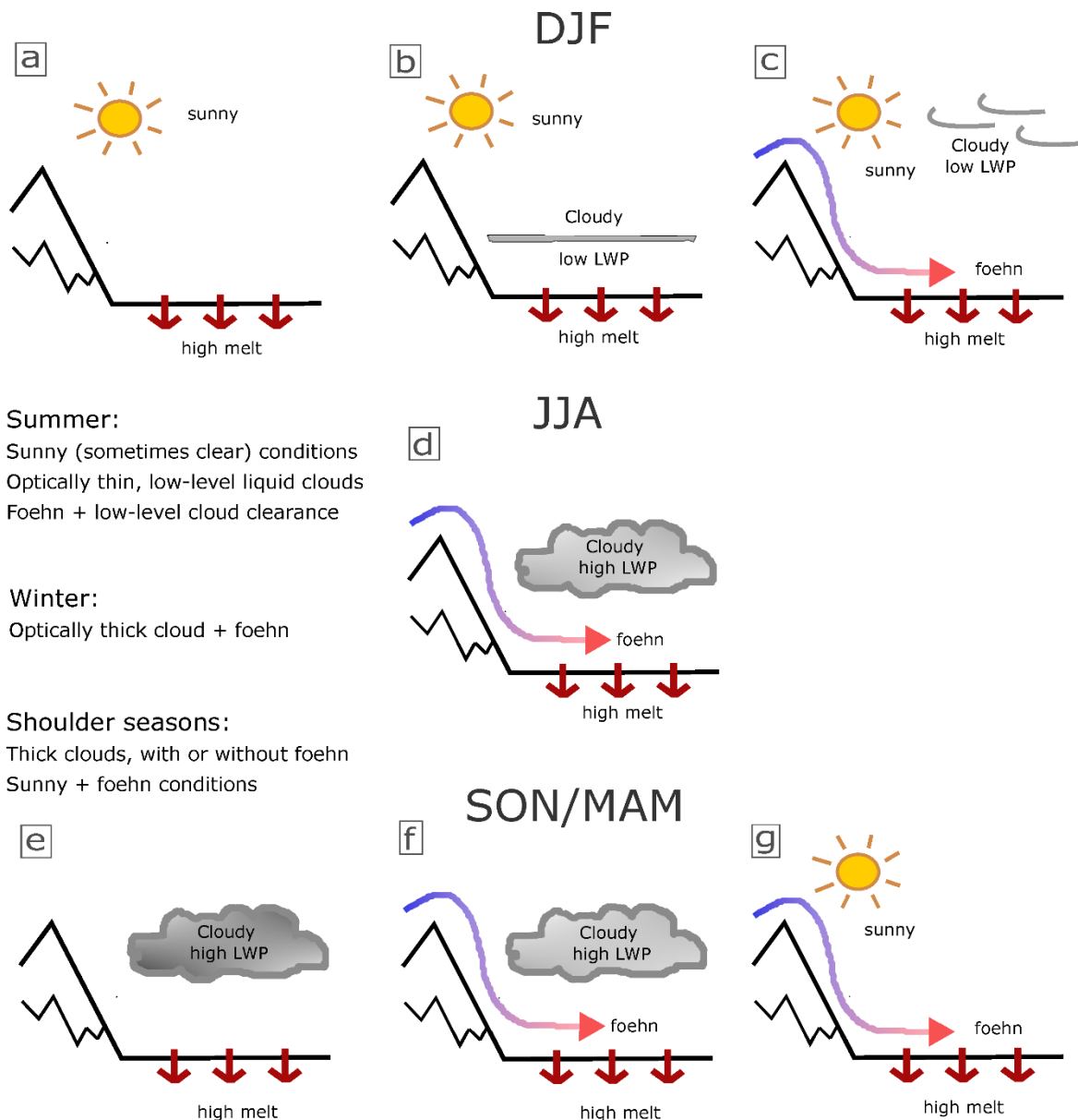
613

614 In DJF, when the majority of melting occurs, E_{melt} anomalies averaged across the whole ice
615 shelf are positive during ‘sunny foehn’, ‘low LWP foehn’ and ‘clear foehn’ (1.00, 0.70 and
616 0.62 W m^{-2} , respectively, Table S1), and near-zero or negative during ‘cloudy foehn’ and
617 ‘high LWP foehn’ (0.02 and -0.32 W m^{-2} , respectively, Table S1). In other seasons the largest
618 positive E_{melt} anomalies are associated with cloudy foehn and high LWP foehn (1.02 and 2.03
619 W m^{-2} , respectively in MAM and 0.31 and 0.54 W m^{-2} , respectively in SON, Table S1,
620 Figure 5f).

621

622 Periods when all three criteria (‘clear foehn’, ‘low LWP foehn’ and ‘sunny foehn’) all occur
623 together are uncommon, happening during <1% of the hindcast. However, these periods
624 coincide with 1-4% of high melt periods (not shown), implying that foehn-induced cloud
625 clearance may drive above-average summertime melt when it occurs, but that such conditions
626 occur fairly infrequently. Further examination of the importance of foehn clearance is needed
627 to comprehensively evaluate its role in driving melt.

628



629

630 **Figure 5.** Schematic diagram illustrating the co-occurrence of various conditions and
 631 dominant modes of melting during each season. Note that melting in JJA occurs extremely
 632 infrequently and is associated with very small E_{melt} fluxes when it does occur.

633

634 3.2.5 The influence of large-scale circulation

635

636 While the most important first-order processes driving surface melting are SW radiation,
 637 foehn and cloud, large-scale circulation variations - associated with patterns like the SAM,
 638 ENSO and ASL - exert controls on these processes. For example, the high melt years
 639 identified in Part 1 were also SAM+ years, supporting the idea that this atmospheric
 640 circulation pattern enhances melting. Table 2 suggests that SAM+ and ENSO- enhance

641 surface melting in DJF and MAM, because the percentage of melt that is associated with
642 them is higher than the percentage of time they occur. Meanwhile SAM-, ENSO+ and ASL
643 conditions suppress melting in all seasons except for ENSO+ in SON (Table 2). This anti-
644 correlation of ENSO/SAM modes (i.e. the co-occurrence of ENSO- and SAM+ conditions
645 and vice versa) is consistent with the findings of e.g. Fogt et al. (2011) and Dätwyler et al.
646 (2020) noted in section 1. As discussed in section 1, ASL conditions strengthen the flow
647 impinging on the Antarctic Peninsula and so can increase the advection of air over the
648 peninsula mountains (Hosking et al., 2013), therefore enhancing melt over Larsen C.

649

650 Figure 6 shows composited mean meteorological conditions and E_{melt} anomalies during
651 SAM+, SAM-, ENSO+, ENSO-, barrier wind and ASL conditions. Anomalies are shown for
652 DJF only, when their absolute influence on E_{melt} is strongest, although they have a larger
653 relative effect on circulation and melting in other seasons. Comparing panels 6d and 6j
654 further confirms that SAM+ and SAM- conditions produce positive and negative E_{melt}
655 anomalies, respectively, especially in the immediate lee of steep terrain. Figure 6c and 6e also
656 show that the circulation patterns in DJF associated with SAM+ and ENSO- are very similar,
657 with weak cyclonic flow west of the Antarctic Peninsula generating weak cross-peninsula
658 flow across Larsen C. This similarity is consistent with the anti-correlation between ENSO
659 and SAM modes previously noted (Fogt et al., 2011; Dätwyler et al., 2020). T_{max} anomalies in
660 Figure 6c and 6e are close to zero, suggesting that SAM+ and ENSO- produce positive melt
661 anomalies (Figure 6d, f) via their effect on the SEB, rather than because they raise
662 temperatures. During SAM+ and ENSO- conditions in DJF, the SEB is dominated by SW_{\downarrow} ,
663 which causes surface melting to be widespread across the ice shelf. The synoptic conditions
664 associated with SAM+ and ENSO- are more extreme during MAM (not shown), when
665 intensive foehn conditions are common (as shown above), and generate positive T_{max} , H_S and
666 E_{melt} anomalies in inlets.

667

668 As shown in Table 2 and Figure 6a and 6b, (deep) ASL conditions are associated with
669 positive T_{max} and E_{melt} anomalies over Larsen C during DJF and MAM. However, whereas in
670 DJF ASL conditions are associated with positive E_{melt} anomalies across the entire shelf
671 (Figure 6b), in MAM (not shown) the anomalies are confined to inlets with a similar pattern
672 to the foehn composite shown in Figure 3q. Conversely, during SON and JJA ASL conditions
673 are associated with negative T_{max} anomalies and in SON with slightly negative E_{melt}
674 anomalies (not shown). Therefore, despite occurring 36.6% and 11.6% of the time, ASL

675 conditions are associated with just 19.4% and 0.2% of melting during SON and JJA,
676 respectively (Table 2).

677

678 These conditions are non-independent and the similarities between them further suggest that
679 SAM+, ENSO- and (in some seasons) ASL patterns produce flow-over conditions that result
680 in foehn, the importance of which has been demonstrated. The co-occurrence of foehn and
681 SAM+ or ENSO- conditions can also be used to demonstrate the influence of large-scale
682 circulation patterns on mesoscale meteorology. Of the times when foehn conditions are
683 detected, SAM+ conditions also occur 26%, 37%, 23% and 28% of the time for SON, DJF,
684 MAM and JJA, respectively, while ENSO- coincides with foehn conditions 24%, 32%, 35%
685 and 17% of the time, respectively. This suggests that SAM+ is most important for
686 establishing foehn conditions during DJF while ENSO- is most influential in MAM.

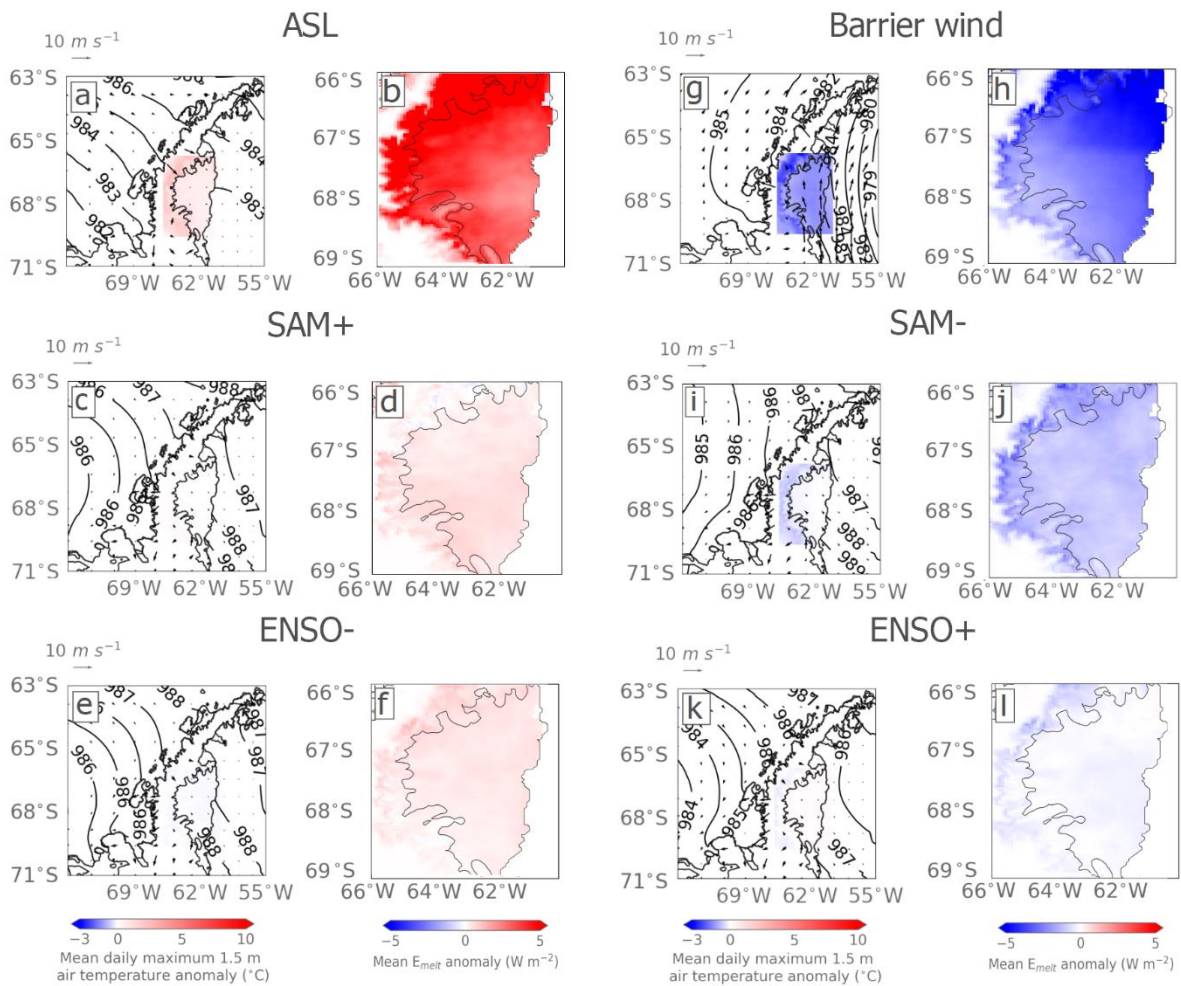
687

688 SAM+ has been more robustly linked to foehn occurrence, and its importance is supported by
689 the results presented in Table 5, which shows Pearson correlation coefficients between
690 observed SAM index and modelled foehn wind frequency at inlet and ice shelf stations for all
691 seasons and annually, and Figure 7, which shows the relationship between these variables at
692 inlet stations only. The correlation between annually averaged SAM index and annual mean
693 foehn frequency is 0.52 in inlets and 0.54 at over the ice shelf (both significant at the 95%
694 level, Table 5). This suggests that a more positive SAM index corresponds to periods of
695 higher foehn occurrence, as also shown by e.g. Cape et al. (2015). The largest and most
696 significant Pearson correlation coefficient between seasonal mean SAM index and foehn
697 occurrence (at the 99% level) is found during DJF, while it is weakest (and insignificant)
698 during JJA. Meanwhile, those correlations in SON and MAM are significant at the 95% level
699 (Table 5).

700

701 The composites presented in Figure 6 and the correlations between SAM+ and foehn
702 conditions in Table 5 and Figure 7 demonstrate the importance of large-scale atmospheric
703 circulation patterns in establishing mesoscale atmospheric conditions like foehn that promote
704 surface melting on Larsen C.

705



706

707 **Figure 6.** Composites synoptic conditions and mean E_{melt} anomalies for the large-scale
 708 circulation patterns: ASL (a, b), SAM+ (c, d), ENSO- (e, f), barrier winds (g, h), SAM- (i, j),
 709 and ENSO+ (k, l). Composites are shown for DJF only, when the absolute effect on E_{melt} is
 710 largest. Conditions that enhance melt are shown in panels a-f, while conditions that suppress
 711 melt are shown in panels g-l. Colours, vectors and contours are as in previous figures.

712

713

714

715

716

717

718

719

720

721

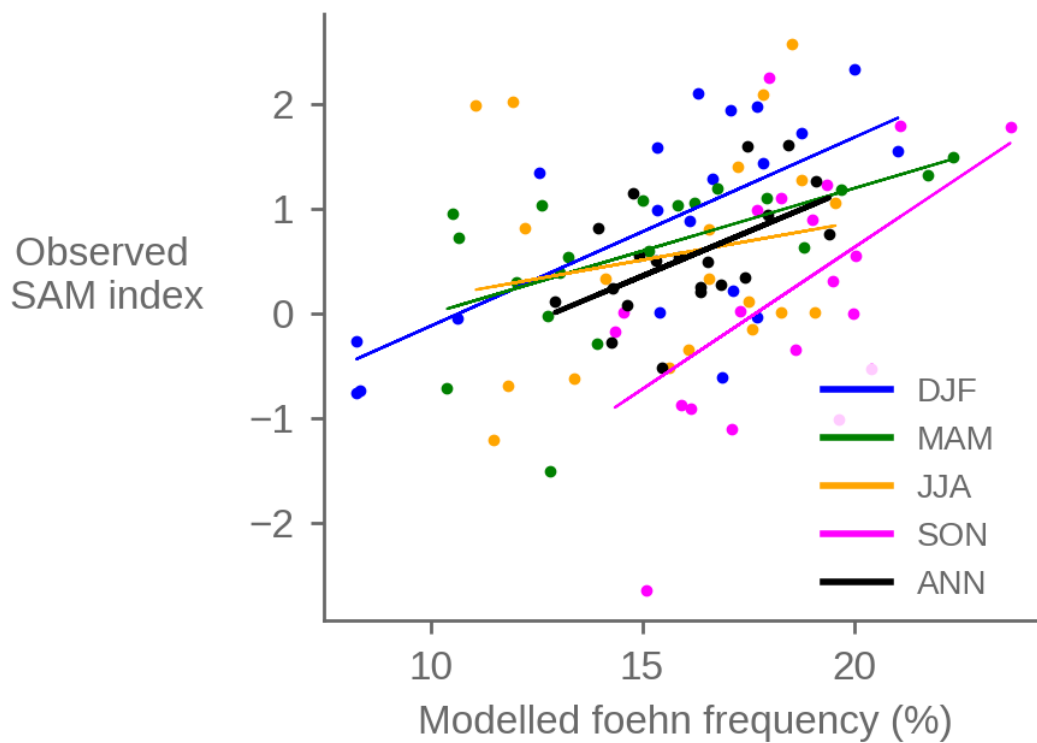
722 **Table 5.** Pearson correlation coefficients between modelled foehn frequency at inlet and ice
 723 shelf stations with the observed SAM index for the duration of the hindcast. Correlations that
 724 are statistically significant at the 95% level are given in bold, while statistical significance of
 725 99% is indicated with an asterisk.

726

Season	Inlet	Ice shelf
DJF	0.66*	0.62*
MAM	0.55	0.54
JJA	0.19	0.16
SON	0.50	0.46
ANN	0.52	0.54

727

728



729

730 **Figure 7.** Scatter plot of hindcast modelled seasonal mean foehn occurrence at inlet stations,
 731 expressed as a percentage of time, against observed seasonal mean SAM index for the
 732 duration of the hindcast, calculated after Marshall (2003). Individual seasons are shown with
 733 coloured markers and the regression line for each season is shown in the corresponding
 734 colour. The annual mean is indicated with black markers and the solid black line.

735 SAM and ENSO may also influence the SEB and melting via their impact on cloudiness. As
736 noted in section 3.2.4, foehn events can be associated with cloud clearance in some
737 situations, and so it follows from the link between SAM+ (and by extension ENSO-)
738 conditions and foehn occurrence that these large-scale circulation patterns could reduce cloud
739 cover. Indeed, SAM+/ENSO- conditions are associated with negative LW_{net} anomalies and
740 positive SW_{net} and H_s anomalies (not shown), suggesting that these conditions are associated
741 with reduced cloud cover or thickness as well as foehn conditions. Meanwhile, during all
742 seasons, SAM-/ENSO+ conditions are associated with the same conditions that increase
743 cloudiness over Larsen C – notably the southeasterly flow of maritime air from over the
744 Weddell Sea. As described in section 3.2.3, this southeasterly airflow can enhance cloud
745 cover and thickness, reduce SW_{\downarrow} and T_{max} , and consequently suppress E_{melt} .

746

747 3.2.6 Conditions that suppress melt

748

749 The focus of this study has been on conditions that enhance surface melting. However, it is
750 evident from Table 2 and Figure 6 that some atmospheric conditions suppress melting, most
751 notably barrier wind, SAM- and ENSO+ conditions. Low melt periods (melt amount < 25th
752 percentile) in DJF are associated with the development of a southerly barrier jet that delivers
753 cold air from high on the Antarctic plateau, typically established by cyclones in the Weddell
754 Sea that produce coastal easterlies or south-easterlies, resulting in cold T_{max} anomalies over
755 Larsen C (not shown). Barrier wind conditions are associated with extremely negative T_{max}
756 and E_{melt} anomalies across the entire Larsen C ice shelf (Figure 6g, h). The temperature
757 anomalies are the primary reason that surface melting is suppressed during these periods,
758 because E_{tot} is affected minimally (anomalies are small). SAM- (Figure 6i, j) and ENSO+
759 conditions (Figure 6k, l) also suppress melting relative to DJF climatology because both
760 reduce the flow of air over the peninsula.

761

762 For all three types of melt-suppressing conditions, the magnitude of the simulated negative
763 T_{max} anomalies is greater in non-summer seasons, but E_{melt} anomalies are smaller because the
764 majority of melting occurs in DJF. For instance, in non-summer seasons ENSO+ and SAM-
765 conditions are associated with more southerly flow which brings cold continental air over
766 Larsen C, suppressing temperatures and melting. The exception is ENSO- conditions in SON:
767 during these periods small positive T_{max} anomalies are simulated, which drives a very weak
768 positive E_{melt} anomaly.

769

770 **4 Summary & conclusions**

771

772 This study has comprehensively evaluated the dominant causes of surface melting on the
773 Larsen C ice shelf in a hindcast simulation of two recent decades. Building on previous work
774 that has explored the causes of melt on Larsen C (such as King et al., 2017; Kuipers Munneke
775 et al., 2018; Datta et al., 2019; Wiesenekker et al., 2019; Elvidge et al., 2020 and Gilbert et al.,
776 2020; 2022), this study has systematically ranked the conditions that drive surface melt in
777 order of importance. Many of these conditions overlap and co-occur, and so can reinforce or
778 counteract each other (Figures 4 and 5). However, the analysis presented here has attempted
779 to isolate the effects of individual drivers of surface melting on Larsen C. The most important
780 drivers can be summarised as follows.

781

782 Firstly, SW radiation is the most important driver of melting in DJF, when 90% of melting
783 occurs. Sunny summertime conditions are associated with the highest E_{melt} anomalies of all
784 drivers (Table 2, Figure 3).

785

786 Secondly, foehn winds are the most important driver of melt in non-summer seasons,
787 especially MAM, but non-summer melt only accounts for 10% of annual meltwater
788 production (Table 2, Figure 3). Foehn winds are also important in DJF because they enhance
789 already-high melt fluxes, but their influence is secondary to that of SW_{\downarrow} in summer. E_{melt}
790 anomalies are highest in all seasons when sunny and foehn conditions co-occur (Figure 4).
791 Foehn-induced cloud clearance may drive large E_{melt} anomalies but this occurs relatively
792 infrequently in the hindcast: rather, the occurrence of foehn during already sunny conditions
793 enhances surface melting (Table 4).

794

795 Thirdly, clouds - especially those with high LWP - increase LW_{\downarrow} radiation and therefore E_{tot} .
796 However, because temperatures are typically just below the melting point during cloudy
797 conditions, widespread melting does not regularly occur unless temperatures are already
798 unusually high (Figure 3). This finding has important ramifications. If ongoing atmospheric
799 warming persists, as projected throughout the 21st century, cloud-mediated melting such as is
800 already observed in Greenland and West Antarctica could begin to occur across Larsen C and
801 other ice shelves on the Antarctic Peninsula.

802

803 Finally, large-scale circulation patterns influence regional and mesoscale meteorology by
804 establishing dominant flow regimes. Large-scale patterns such as SAM and ENSO as well as
805 regional features such as the ASL and barrier winds influence atmospheric circulation in the
806 region and can affect the surface meteorology, SEB and melt (Figure 6). Further, large-scale
807 circulation patterns can affect sea ice conditions, which can in turn interact with regional
808 meteorology, for instance moderating the properties of air that flows onto the Larsen C ice
809 shelf.

810

811 Modelled foehn frequency is shown to be strongly correlated with an observed SAM index (r
812 = 0.62, Table 5, Figure 7), which suggests that more foehn events, and therefore more
813 melting, could result if the trend towards a more positive SAM that was recorded from the
814 1960-2000s (Marshall, 2003; Fogt & Marshall, 2020) resumed. While no trends in foehn
815 frequency are evident over the hindcast period, this is likely because we only have 20 years
816 of data and there is considerable interannual variability (c.f. Gilbert et al. 2022).

817

818 The trend towards a more positive SAM is expected to resume as greenhouse gas
819 concentrations increase. Rising greenhouse gas concentrations cause the westerly winds
820 associated with SAM+ to strengthen and migrate polewards and will likely outweigh the
821 compensating effects of ozone recovery if emissions continue at current levels (Zheng et al.,
822 2013). Although future changes to ENSO are highly uncertain (Fredriksen et al., 2020), the
823 coupling between ENSO and SAM may also imply a transition towards ENSO- conditions as
824 the positive SAM trend continues. The combination of higher foehn frequency associated
825 with a more positive SAM and rising temperatures related to ongoing global climate change
826 could contribute to greater meltwater production by allowing melt to occur more frequently
827 via the mechanisms outlined above, and for that melt to be more intense. This could lead to
828 an eventual destabilisation of Larsen C via hydrofracturing, with far-reaching implications
829 for global sea level rise. Larsen C has already been identified as an ice shelf at risk of
830 hydrofracturing-induced collapse if warming continues unchecked (Trusel et al., 2015;
831 Gilbert & Kittel, 2021). Quantifying the future fate of the Larsen C ice shelf is beyond the
832 scope of this paper but should be a focus of research to determine change on the Antarctic
833 Peninsula.

834

835

836

837 **Acknowledgments**

838 The authors declare no conflicts of interest. This work was supported by the Natural
839 Environment Research Council through the EnvEast Doctoral Training Partnership (grant
840 number NE/L002582/1). The authors also acknowledge use of the MONSooN system, a
841 collaborative facility supplied under the Joint Weather and Climate Research Programme, a
842 strategic partnership between the Met Office and the Natural Environment Research Council.
843 The authors gratefully acknowledge Prof. Michiel R. van den Broeke, who kindly provided
844 AWS data.

845 Hindcast model data can be accessed on the CEDA archive at
846 <https://catalogue.ceda.ac.uk/uuid/41c879b06af642e9bc8e12d1d0ea3d62> and can be cited as
847 Gilbert, E. (2020): High-resolution regional Met Office Unified Model (UM) climate model
848 hindcast of the Antarctic Peninsula (1998-2017). Centre for Environmental Data Analysis,
849 date of citation. AWS data can be retrieved from
850 <https://www.projects.science.uu.nl/iceclimate/aws/>.

851 The authors are grateful to R. T. Datta and one anonymous reviewer for helpful
852 comments on an earlier version of this manuscript.

853
854
855
856
857
858
859
860
861
862
863
864
865
866
867
868
869

870

871 **References**

872

873 Bell, R. E., Banwell, A. F., Trusel, L. D., & Kingslake, J. (2018). Antarctic surface hydrology
874 and impacts on ice-sheet mass balance. *Nature Climate Change*, 8(December), 1044–1052.

875 <https://doi.org/10.1038/s41558-018-0326-3>

876

877 Bennartz, R., Shupe, M. D., Turner, D. D., Walden, V. P., Steffen, K., Cox, C. J., Kulie, M.
878 S., Miller, N. B., & Pettersen, C. (2013). July 2012 Greenland melt extent enhanced by low-
879 level liquid clouds. *Nature*, 496(7443), 83–86. <https://doi.org/10.1038/nature12002>

880

881 Bevan, S. L., Luckman, A. J., Kuipers Munneke, P., Hubbard, B., Kulesa, B., & Ashmore,
882 D. W. (2018). Decline in Surface Melt Duration on Larsen C Ice Shelf Revealed by The
883 Advanced Scatterometer (ASCAT). *Earth and Space Science*, 5(10), 578–591.

884 <https://doi.org/10.1029/2018EA000421>

885

886 Bozkurt, D., Bromwich, D. H., Carrasco, J., Hines, K. M., Maureira, J. C., & Rondanelli, R.
887 (2020). Recent Near-surface Temperature Trends in the Antarctic Peninsula from Observed,
888 Reanalysis and Regional Climate Model Data. *Advances in Atmospheric Sciences*, 37, 477–

889 493. <https://doi.org/10.1007/s00376-020-9183-x>

890

891 Cape, M. R., Vernet, M., Skvarca, P., Marinsek, S., Scambos, T., & Domack, E. (2015).
892 Foehn winds link climate-driven warming to ice shelf evolution in Antarctica. *Journal of*
893 *Geophysical Research: Atmospheres*, 120(21), 11037–11057.

894 <https://doi.org/10.1002/2015JD023465>

895

896 Center for Climate Prediction (2005). Teleconnection pattern calculation procedures.

897 https://www.cpc.ncep.noaa.gov/products/precip/CWlink/daily_ao_index/history/method.shtml
898 [I retrieved November 14th 2019.](https://www.cpc.ncep.noaa.gov/products/precip/CWlink/daily_ao_index/history/method.shtml)

899

900 Clem, K. R., Renwick, J. A., McGregor, J., & Fogt, R. L. (2016). The relative influence of
901 ENSO and SAM on Antarctic Peninsula climate. *Journal of Geophysical Research:*

902 *Atmospheres*, 121, 11038–11054. <https://doi.org/10.1002/2016JD02495>

903

904 Datta, R. T., Tedesco, M., Fettweis, X., Agosta, C., Lhermitte, S., Lenaerts, J. T. M., &
905 Wever, N. (2019). The Effect of Foehn-Induced Surface Melt on Firn Evolution Over the
906 Northeast Antarctic Peninsula. *Geophysical Research Letters*, 46, 3822–3831.
907 <https://doi.org/10.1029/2018GL080845>
908

909 Dätwyler, C., Grosjean, M., Steiger, N. J., & Neukom, R. (2020). Teleconnections and
910 relationship between ENSO and SAM in reconstructions and models over the past
911 millennium. *Climate of the Past*, 743–756, 743–756. <https://doi.org/10.5194/cp-2019-110>
912

913 Deb, P., Orr, A., Bromwich, D. H., Nicolas, J. P., Turner, J., & Hosking, J. S. (2018).
914 Summer Drivers of Atmospheric Variability Affecting Ice Shelf Thinning in the Amundsen
915 Sea Embayment, West Antarctica. *Geophysical Research Letters*, 45(9), 4124–4133.
916 <https://doi.org/10.1029/2018GL077092>
917

918 Dee, D. P., Uppala, S. M., Simmons, A. J., Berrisford, P., Poli, P., Kobayashi, S., ... &
919 Bechtold, P. (2011). The ERA-Interim reanalysis: Configuration and performance of the data
920 assimilation system. *Quarterly Journal of the Royal Meteorological Society* 137 (656), 553-
921 597. <https://doi.org/10.1002/qj.828>
922

923 Elvidge, A. D., Renfrew, I. A., King, J. C., Orr, A., Lachlan-Cope, T. A., Weeks, M., &
924 Gray, S. L. (2015). Foehn jets over the Larsen C Ice Shelf, Antarctica. *Quarterly Journal of*
925 *the Royal Meteorological Society*, 141(688), 698–713. <https://doi.org/10.1002/qj.2382>
926

927 Elvidge, A. D., Renfrew, I. A., King, J. C., Orr, A., & Lachlan-Cope, T. A. (2016). Foehn
928 warming distributions in nonlinear and linear flow regimes: A focus on the Antarctic
929 Peninsula. *Quarterly Journal of the Royal Meteorological Society*, 142(695), 618–631.
930 <https://doi.org/10.1002/qj.2489>
931

932 Elvidge, A. D., Kuipers Munneke, P., King, J. C., Renfrew, I. A., & Gilbert, E. (2020).
933 Atmospheric drivers of melt on Larsen C Ice Shelf: surface energy budget regimes and the
934 impact of foehn. *Journal of Geophysical Research: Atmospheres*, 125(17), e2020JD032463.
935 <https://doi.org/https://doi.org/10.1029/2020JD032463>
936

937 Fogt, R. L., Bromwich, D. H., & Hines, K. M. (2011). Understanding the SAM influence on
938 the South Pacific ENSO teleconnection. *Climate Dynamics*, 36(7), 1555–1576.
939 <https://doi.org/10.1007/s00382-010-0905-0>
940

941 Fogt, R. L., & Marshall, G. J. (2020). The Southern Annular Mode: Variability, trends, and
942 climate impacts across the Southern Hemisphere. *WIREs Climate Change*, 11(4), e652.
943 <https://doi.org/10.1002/wcc.652>
944

945 Fredriksen, H. B., Berner, J., Subramanian, A. C., & Capotondi, A. (2020). How Does El
946 Niño–Southern Oscillation Change Under Global Warming—A First Look at CMIP6.
947 *Geophysical Research Letters*, 47(22). <https://doi.org/10.1029/2020GL090640>
948

949 Ghiz, M., Scott, R., Vogelmann, A., Lenaerts, J., Lazzara, M., & Lubin, D. (2021).
950 Energetics of Surface Melt in West Antarctica. *The Cryosphere*, 15, 3459–3494.
951 <https://doi.org/https://doi.org/10.5194/tc-15-3459-2021>
952

953 Gilbert, E. (2020a). High-resolution regional Met Office Unified Model (UM) climate model
954 hindcast of the Antarctic Peninsula (1998-2017). Centre for Environmental Data
955 Analysis, 16/09/2021 available at:
956 <https://catalogue.ceda.ac.uk/uuid/41c879b06af642e9bc8e12d1d0ea3d62>

957 Gilbert, E. (2020b) Atmospheric drivers of surface melting on the Larsen C ice shelf,
958 Antarctic Peninsula. PhD thesis, University of East Anglia.
959

960 Gilbert, E., Orr, A., King, J. C., Renfrew, I. A., Lachlan-Cope, T., Field, P. F., & Boutle, I. A.
961 (2020). Summertime cloud phase strongly influences surface melting on the Larsen C ice
962 shelf, Antarctica. *Quarterly Journal of the Royal Meteorological Society*, 146(729), 1575–
963 1589. <https://doi.org/10.1002/qj.3753>
964

965 Gilbert, E., & Kittel, C. (2021). Surface melt and runoff on Antarctic ice shelves at 1.5°C,
966 2°C and 4°C of future warming. *Geophysical Research Letters*, 48, e2020GL091733.
967 <https://doi.org/10.1029/2020GL091733>
968

969 [Gilbert, E.; Orr, A.; King, J. C.; Renfrew, I. A. & Lachlan-Cope, T. \(2022\) A 20-year study of](#)
970 [melt processes over Larsen C Ice Shelf using a high-resolution regional atmospheric model:](#)
971 [Part 1, Model configuration and validation. Journal of Geophysical Research: Atmospheres](#)
972 [\(in press\).](#)
973

974 Grosvenor, D. P., King, J. C., Choularton, T. W., & Lachlan-Cope, T. (2014). Downslope
975 foehn winds over the antarctic peninsula and their effect on the larsen ice shelves.
976 *Atmospheric Chemistry and Physics*, 14(18), 9481–9509. [https://doi.org/10.5194/acp-14-](https://doi.org/10.5194/acp-14-9481-2014)
977 [9481-2014](https://doi.org/10.5194/acp-14-9481-2014)
978

979 Hofer, S., Tedstone, A.J., Fettweis, X. & Bamber, J. (2019) Cloud microphysics and
980 circulation anomalies control differences in future Greenland melt. *Nature Climate*
981 *Change* 9, 523–528 <https://doi.org/10.1038/s41558-019-0507-8>
982

983 Hoinka, K. P. (1985). What is a Foehn Clearance? *Bulletin of the American Meteorological*
984 *Society*, 66(9), 1123–1132. [https://doi.org/10.1175/1520-](https://doi.org/10.1175/1520-0477(1985)066%3C1123:WIAFC%3E2.0.CO;2)
985 [0477\(1985\)066%3C1123:WIAFC%3E2.0.CO;2](https://doi.org/10.1175/1520-0477(1985)066%3C1123:WIAFC%3E2.0.CO;2)
986

987 Hosking, J. S., Orr, A., Marshall, G. J., Turner, J., & Phillips, T. (2013). The influence of the
988 amundsen-bellingshausen seas low on the climate of West Antarctica and its representation in
989 coupled climate model simulations. *Journal of Climate*, 26(17), 6633–6648.
990 <https://doi.org/10.1175/JCLI-D-12-00813.1>
991

992 King, J. C. (1994) Recent climate variability in the vicinity of the Antarctic
993 Peninsula. *International Journal of Climatology*, 14, 357–369,
994 <https://doi.org/10.1002/joc.3370140402>
995

996 King, J. C., Gadian, A., Kirchgassner, A., Kuipers Munneke, P., Lachlan-Cope, T. A., Orr,
997 A., Reijmer, C., Van Den Broeke, M. R., Van Wessem, J. M., & Weeks, M. (2015).
998 Validation of the summertime surface energy budget of Larsen C Ice Shelf (Antarctica) as
999 represented in three high-resolution atmospheric models. *Journal of Geophysical Research*
1000 *Atmospheres*, 120(4), 1335–1347. <https://doi.org/10.1002/2014JD022604>
1001

1002 King, J. C., Kirchgaessner, A., Orr, A., Luckman, A., Bevan, S., Elvidge, A., Renfrew, I. A.,
1003 & Kuipers Munneke, P. (2017). The impact of foehn winds on surface energy balance and
1004 melt over Larsen C Ice Shelf, Antarctica. *Journal of Geophysical Research: Atmospheres*,
1005 122(22), 12062–12076. <https://doi.org/10.1002/2017JD026809>
1006

1007 Kuipers Munneke, P., Van Den Broeke, M. R., King, J. C., Gray, T., & Reijmer, C. H.
1008 (2012). Near-surface climate and surface energy budget of Larsen C ice shelf, Antarctic
1009 Peninsula. *Cryosphere*, 6(2), 353–363. <https://doi.org/10.5194/tc-6-353-2012>
1010

1011 Kuipers Munneke, P., Luckman, A. J., Bevan, S. L., Gilbert, E., Smeets, C. J. P. P., Van Den
1012 Broeke, M. R., Wang, W., Zender, C., Hubbard, B., Ashmore, D., Orr, A., & King, J. C.
1013 (2018). Intense winter surface melt on an Antarctic ice shelf. *Geophysical Research Letters*,
1014 45, 7615–7623. <https://doi.org/10.1029/2018GL077899>
1015

1016 Laffin, M. K., Zender, C. S., Singh, S., Van Wessem, J. M., Smeets, C. J. P. P., & Reijmer,
1017 C. H. (2021). Climatology and Evolution of the Antarctic Peninsula Föhn Wind-Induced Melt
1018 Regime From 1979–2018. *Journal of Geophysical Research: Atmospheres*, 126(4), 1–19.
1019 <https://doi.org/10.1029/2020JD033682>
1020

1021 Lai, C. Y., Kingslake, J., Wearing, M. G., Chen, P. H. C., Gentine, P., Li, H., Spergel, J. J., &
1022 van Wessem, J. M. (2020). Vulnerability of Antarctica’s ice shelves to meltwater-driven
1023 fracture. *Nature*, 584(7822), 574–578. <https://doi.org/10.1038/s41586-020-2627-8>
1024

1025 Liu, H., Jezek, K. C., Li, B., & Zhao, Z. (2015). RadarSat Antarctic Mapping Project Digital
1026 Elevation Model, version 2. NSIDC; NASA National Snow and Ice Data Center Distributed
1027 Active Archive Center. <https://doi.org/https://doi.org/10.5067/8JKNEW6BFRVD>
1028

1029 Marshall, G. J. (2003). Trends in the Southern Annular Mode from observations and
1030 reanalyses. *Journal of Climate*, 16(24), 4134–4143. [https://doi.org/10.1175/1520-
1031 0442\(2003\)016<4134:TITSAM>2.0.CO;2](https://doi.org/10.1175/1520-0442(2003)016<4134:TITSAM>2.0.CO;2)
1032

1033 Marshall, G. J., Orr, A., van é, N. P. M., & King, J. C. (2006). The impact of a changing
1034 Southern Hemisphere Annular Mode on Antarctic Peninsula summer temperatures. *Journal of*
1035 *Climate*, 19(20), 5388–5404. <https://doi.org/10.1175/JCLI3844.1>

1036
1037 Orr, A., D. Cresswell, G. J. Marshall, J. C. R. Hunt, J. Sommeria, and C. G. Wang (2004), A
1038 ‘low-level’ explanation for the recent large warming trend over the western Antarctic
1039 Peninsula involving blocked winds and changes in zonal circulation, *Geophysical Research*
1040 *Letters* 31, L06204, <https://doi.org/10.1029/2003GL019160>.
1041
1042 Orr, A., Marshall, G. J., Hunt, J. C. R., Sommeria, J., Wang, C.-G., van Lipzig, N. P. M.,
1043 Cresswell, D., & King, J. C. (2008). Characteristics of Summer Airflow over the Antarctic
1044 Peninsula in Response to Recent Strengthening of Westerly Circumpolar Winds. *Journal of*
1045 *the Atmospheric Sciences* 65 (4), 1396–1413. <https://doi.org/10.1175/2007JAS2498.1>
1046
1047 Orr, A., A. Kirchgaessner, J. King, T. Phillips, E. Gilbert, A. Elvidge, M. Weeks, A. Gadian,
1048 P. Kuipers Munneke, M. van den Broeke, S. Webster, and D. McGrath (2021), Comparison
1049 of kilometre and sub-kilometre scale simulations of a foehn wind event over the Larsen C Ice
1050 Shelf using the Met Office Unified Model (MetUM), *Quarterly Journal of the Royal*
1051 *Meteorological Society*, <https://doi.org/10.1002/qj.4138>
1052
1053 Parish, T. R. (1983) The influence of the Antarctic Peninsula on the wind field over the
1054 western Weddell Sea. *Journal of Geophysical Research*, **88**, 2684–2692,
1055 <https://doi.org/10.1029/JC088iC04p02684>
1056
1057 Reynolds, R. W., Smith, T. M., Liu, C., Chelton, D. B., Casey, K. S., & Schlax, M. G.
1058 (2007). Daily high-resolution-blended analyses for sea surface temperature. *Journal of*
1059 *Climate*, 20 (22), 5473–5496. <https://doi.org/10.1175/2007JCLI1824.1>
1060
1061 Scambos, T. A., Hulbe, C., Fahnestock, M. & Bohlander, J. (2000). The link between climate
1062 warming and break-up of ice shelves in the Antarctica Peninsula. *Journal of Glaciology*,
1063 46(154), 516–530. <https://doi.org/10.3189/172756500781833043>
1064
1065 Scambos, T., Hulbe, C., & Fahnestock, M. (2003). Climate-induced ice shelf disintegration in
1066 the Antarctic Peninsula. In E. Domack, A. Levente, A. Burnet, R. Bindshadler, P. Convey,
1067 & M. Kirby (Eds.), *Antarctic Peninsula Climate Variability: Historical and*
1068 *Paleoenvironmental Perspectives* (Vol. 79, pp. 79–92).
1069 <https://doi.org/doi:10.1029/AR079p0079>

1070

1071 Schwerdtfeger, W., (1975). The effect of the Antarctic Peninsula on the temperature regime
1072 of the Weddell Sea. *Monthly Weather Review* 103, 45–51, [https://doi.org/10.1175/1520-
1073 0493\(1975\)103<0045:TEOTAP>2.0.CO;2](https://doi.org/10.1175/1520-0493(1975)103<0045:TEOTAP>2.0.CO;2)

1074

1075 Siegert, M., Atkinson, A., Banwell, A., Brandon, M., Convey, P., Davies, B., Downie, R.,
1076 Edwards, T., Hubbard, B., Marshall, G., Rogelj, J., Rumble, J., Stroeve, J., & Vaughan, D.
1077 (2019). The Antarctic Peninsula under a 1.5°C global warming scenario. *Frontiers in
1078 Environmental Science*, 7(JUN), 1–7. <https://doi.org/10.3389/fenvs.2019.00102>

1079

1080 Takane, Y., & Kusaka, H. (2011). Formation mechanisms of the extreme high surface air
1081 temperature of 40.9°C observed in the Tokyo metropolitan area: Considerations of dynamic
1082 foehn and foehnlike wind. *Journal of Applied Meteorology and Climatology*, 50(9), 1827–
1083 1841. <https://doi.org/10.1175/JAMC-D-10-05032.1>

1084

1085 Trusel, L. D., Frey, K. E., Das, S. B., Karnauskas, K. B., Kuipers Munneke, P., van
1086 Meijgaard, E., & van den Broeke, M. R. (2015). Divergent trajectories of Antarctic surface
1087 melt under two twenty-first-century climate scenarios. *Nature Geoscience*, 8(12), 927–932.
1088 <https://doi.org/10.1038/ngeo2563>

1089

1090 Turner, J., Phillips, T., Hosking, J. S., Marshall, G. J., & Orr, A. (2013). The Amundsen sea
1091 low. *International Journal of Climatology*, 33(7), 1818–1829.
1092 <https://doi.org/10.1002/joc.3558>

1093

1094 Turton, J. V., Kirchgaessner, A., Ross, A. N., & King, J. C. (2018). The spatial distribution
1095 and temporal variability of föhn winds over the Larsen C ice shelf, Antarctica. *Quarterly
1096 Journal of the Royal Meteorological Society*, 144(713), 1169–1178.
1097 <https://doi.org/10.1002/qj.3284>

1098

1099 Turton, J. V., Kirchgaessner, A., Ross, A., King, J., & Kuipers Munneke, P. (2020). The
1100 influence of föhn winds on annual and seasonal surface melt on the Larsen C Ice Shelf,
1101 Antarctica. *The Cryosphere Discussions*, 14, 4165–4180. <https://doi.org/10.5194/tc-2020-72>

1102

1103 van Lipzig, N. P. M., Marshall, G. J., Orr, A., & King, J. C. (2008). The relationship between
1104 the Southern Hemisphere annular mode and Antarctic Peninsula summer temperatures:
1105 Analysis of a high-resolution model climatology. *Journal of Climate* 21 (8), 1649–1668.
1106 <https://doi.org/10.1175/2007JCLI1695.1>
1107
1108 van Oldenborgh, G. J., Collins, M., Arblaster, J., Christensen, J. H., Marotzke, J., Power, S.
1109 B., Rummukainen, M., & Zhou, T. (Eds. . (2013). Atlas of Global and Regional Climate
1110 Projections. In T. F. Stocker, D. Qin, G.-K. Plattner, M. Tignor, S. K. Allen, J. Boschung, A.
1111 Nauels, Y. Xia, V. Bex, & P. M. Midgley (Eds.), *Climate Change 2013: The Physical*
1112 *Science Basis. Contribution of Working Group I to the Fifth Assessment Report of the*
1113 *Intergovernmental Panel on Climate Change*. Cambridge University Press.
1114 <https://doi.org/http://dx.doi.org/10.1017/CBO9781107415324.029>
1115
1116 Van Wessem, J. M., Reijmer, C. H., Van De Berg, W. J., Van Den Broeke, M. R., Cook, A.
1117 J., Van Uft, L. H., & Van Meijgaard, E. (2015). Temperature and wind climate of the
1118 Antarctic Peninsula as simulated by a high-resolution Regional Atmospheric Climate Model.
1119 *Journal of Climate*, 28(18), 7306–7326. <https://doi.org/10.1175/JCLI-D-15-0060.1>
1120
1121 Van Wessem, J. M., Ligtenberg, S. R. M., Reijmer, C. H., Van De Berg, W. J., Van Den
1122 Broeke, M. R., Barrand, N. E., Thomas, E. R., Turner, J., Wuite, J., Scambos, T. A., & Van
1123 Meijgaard, E. (2016). The modelled surface mass balance of the Antarctic Peninsula at 5.5
1124 km horizontal resolution. *Cryosphere*, 10(1), 271–285. [https://doi.org/10.5194/tc-10-271-](https://doi.org/10.5194/tc-10-271-2016)
1125 [2016](https://doi.org/10.5194/tc-10-271-2016)
1126
1127 Wiesenekker, J. M., Munneke, P. K., van den Broeke, M. R., & Paul Smeets, C. J. P. (2018).
1128 A multidecadal analysis of Föhn winds over Larsen C ice shelf from a combination of
1129 observations and modeling. *Atmosphere*, 9(5). <https://doi.org/10.3390/atmos9050172>
1130
1131 Zhang, T., Stamnes, K., & Bowling, S. A. (1996). Impact of Clouds on Surface Radiative
1132 Fluxes and Snowmelt in the Arctic and Subarctic. *Journal of Climate*, 9(9), 2110–2123.
1133 [https://doi.org/10.1175/1520-0442\(1996\)009<2110:IOCOSR>2.0.CO;2](https://doi.org/10.1175/1520-0442(1996)009<2110:IOCOSR>2.0.CO;2)
1134

1135 Zheng, F., Li, J., Clark, R. T., & Nnamchi, H. C. (2013). Simulation and projection of the
1136 Southern Hemisphere annular mode in CMIP5 models. *Journal of Climate*, 26(24), 9860–
1137 9879. <https://doi.org/10.1175/JCLI-D-13-00204.1>